Collective rotational transverse current multipoles: Even-even nuclei

D. Berdichevsky,* P. Sarriguren, E. Moya de Guerra,† M. Nishimura,‡ and D. W. L. Sprung
Department of Physics, McMaster University, Hamilton, Ontario, Canada L8S 4M1
(Received 19 January 1988)

We present a systematic study of transverse current multipoles of the ground-state band in even-even rare-earth nuclei. We analyze the q dependence of the form factors under different assumptions about the nature of the rotational mode. We show and compare numerical results of projected-Hartree-Fock and cranking model calculations for ^{154}Sm, ^{156,158}Gd, ^{164}Dy, ^{166,168}Er, and ^{174}Yb. We discuss the dependence of the multipoles on the mean field used to generate the ground-state wave function. Finally, we compare to predictions of the rigid rotor and irrotational fluid flow models. Comparison to experiment is restricted to very low momentum transfer by lack of relevant data.

I. INTRODUCTION

Understanding the nature of nuclear collective rotation has been a subject of much interest ever since low-lying rotational bands were first observed.[1] In this respect the cranking model has been very useful. It has successfully described moments of inertia and gyromagnetic ratios[2,3] of ground-state bands as well as high-spin states in higher spectral regions.[4] But how nuclei actually rotate is still an open question, and one which has gained new impetus with the recent discovery[5] of a new collective 1^+ excitation called the scissors mode in deformed nuclei of the rare-earth region. Flow patterns which reflect the rotational dynamics have been calculated using the cranking model by several groups.[6] Such calculations are very interesting as they attempt to separate the rotational current into rigid and irrotational flow components plus a residual term which exhibits vortices, but unfortunately these quantities are not measurables.

That models of the collective rotational current could be experimentally verified by measuring transverse form factors in electron scattering was first pointed out in Refs. 7–9. In particular, in Ref. 8 a few results were presented of transverse form factors of even-even and odd-A deformed nuclei computed in the projected-Hartree-Fock (PHF) approximation using the effective interaction derived by Negele and Vautherin[10] by the density-matrix expansion (DME) method. In Ref. 9 predictions of various models were discussed qualitatively and the usefulness of considering transverse inelastic electron scattering to excited states in the ground-state band was emphasized. Indeed, calculations of transverse form factors for the $0^+ \rightarrow 2^+, 4^+$ transitions in ^{166}Er reported in Refs. 11 and 12 showed a strong model dependence. The purpose of this paper is to give a thorough quantitative comparison of predictions of several models concerning the transverse electric and magnetic multipoles of the collective rotational current. To that purpose we consider here the rare-earth nuclei ^{154}Sm, ^{156,158}Gd, ^{164}Dy, ^{166,168}Er, and ^{174}Yb, and four different models (cranking, PHF, rigid rotor and irrotational flow). Our results are shown in q space, to allow for comparison with future experimental data. In this regard, it should be noted that, except at the photon point, experimental values for transverse form factors of even-even nuclear ground-state bands are not yet available. Transverse electric multipoles are expected to be measured soon from backwards (e,e') and coincidence $(e,e'\gamma)$ on even-even nuclei,[13,14] but further information on them can be gained in future from transitions to collective 1^+ bands as well as from magnetic form factors of odd-A nuclei.[15] Obviously, comparison to these future experiments will require taking distortion effects into account.[16] These are not considered in this paper since they would complicate the discussion without illuminating those issues which we address.

This paper is organized as follows: Section II contains a brief summary of theory while Sec. III contains the numerical results. A detailed discussion of the microscopic model calculations is divided between Secs. III B and III C; the former focusses on the problem of numerical convergence while the latter is dedicated to a comparison of the PHF and cranking model results using different mean fields. Convection and magnetization contributions to the form factors are considered separately. Section III D deals with a comparison of the microscopic and macroscopic models, as well as with comparison to experiment at the photon point. Our main results and conclusions are summarized in Sec. IV.

II. BRIEF SUMMARY OF THEORY

The general structure of electromagnetic form factors of axially symmetric deformed nuclei has been presented in Refs. 7, 9, and 17. Here we summarize the main results needed for the present discussion. We follow the conventions and notation of Ref. 17, in particular for the transition and intrinsic multipole form factors, except for a factor of $\sqrt{4\pi}/Z$ which we include in our definition of the form factors.

We denote by $\mathcal{F}_R^{E\lambda}$, $\mathcal{F}_R^{M\lambda}$ the q dependent intrinsic transverse electric and magnetic multipoles of the ground-state band. Then the $E\lambda$ and $M\lambda$ multipole form factors for a given transition within the ground-state

 ©1988 The American Physical Society

$K=0$ band, from an initial state (I_i) to a final nuclear state (I_f) are given by

$$F^{E\lambda}(q)\,|_{I_i\to I_f}=[I_f(I_f+1)-I_i(I_i+1)] \times\langle I_i 0\lambda 0\,|\,I_f 0\rangle \mathcal{F}_R^{E\lambda}(q),\quad \text{even } \lambda\geq 2\ , \tag{1}$$

$$F^{M\lambda}(q)\,|_{I_i\to I_f}=\sqrt{2I_i(I_i+1)}\langle I_i 1\lambda -1\,|\,I_f 0\rangle \times\mathcal{F}_R^{M\lambda}(q),\quad \lambda=\text{odd}\ , \tag{2}$$

where it is clear that the q dependence of the transition multipoles $F^{\sigma\lambda}$ is fully contained in the intrinsic multipoles $\mathcal{F}_R^{\sigma\lambda}$. As discussed in Ref. 17, different rotational models provide different predictions for the intrinsic multipoles. In this paper we focus attention on a comparison of the PHF and cranking models. Then, to first order in components of the total angular momentum operator,[9,17] the intrinsic multipoles are independent of initial and final spins (I_i, I_f), and may be written in compact form as

$$\mathcal{F}_R^{\sigma\lambda}(q)=\frac{\sqrt{4\pi}}{Z}\alpha^{\sigma\lambda}\sum_\nu A_\nu \mathrm{Re}(\langle\nu\,|\,T_1^{\sigma\lambda}(q)\,|\,\phi_0\rangle^* \times\langle\nu\,|\,J_+\,|\,\phi_0\rangle)\ , \tag{3}$$

$$\alpha^{\sigma\lambda}=\begin{cases}-\sqrt{2}, & \sigma=M\\ [\lambda(\lambda+1)]^{-1/2}, & \sigma=E.\end{cases}$$

Here, ϕ_0 is the (time-even) intrinsic deformed ground state in the HF or Hartree-Fock-Bogolyubov (HFB) approximation, and $|\nu\rangle$ represents any excited 1p-1h or two-quasiparticle state connected to ϕ_0 by the raising component of the total angular momentum operator. $T_1^{\sigma\lambda}$ is the $m=1$ component of the $\sigma\lambda$ ($\sigma=E,M$) tensor operator.[17–19] The coefficients A_ν depend on the microscopic model being used: In the PHF approximation they are common to all the intermediate states $|\nu\rangle$, while in the cranking model they depend on the excitation energy of the intermediate state:

$$A_\nu=\begin{cases}1/\langle J_\perp^2\rangle, & \text{in PHF}\\ 1/[\mathcal{I}_{\rm cr}(\epsilon_\nu-\epsilon_0)], & \text{in cranking.}\end{cases} \tag{4}$$

In Eq. (4), $\langle J_\perp^2\rangle$ is the expectation value of the squared angular momentum operator in the intrinsic ground state ϕ_0, $(\epsilon_\nu-\epsilon_0)$ is the excitation energy of state $|\nu\rangle$, and $\mathcal{I}_{\rm cr}$ is the cranking[20] moment of inertia:

$$\langle J_\perp^2\rangle=\langle\phi_0\,|\,J_\perp^2\,|\,\phi_0\rangle=\sum_\nu |\langle\nu\,|\,J_+\,|\,\phi_0\rangle|^2\ , \tag{5}$$

$$\mathcal{I}_{\rm cr}=\sum_\nu |\langle\nu\,|\,J_+\,|\,\phi_0\rangle|^2/(\epsilon_\nu-\epsilon_0)\ . \tag{6}$$

It is then clear that the dependence on initial and final spins of the transition multipoles, as measured in the laboratory frame, is contained in the geometrical factors shown explicitly in Eqs. (1) and (2). Taking into account the properties of Clebsch-Gordan coefficients and the fact that for the ground-state band the spin sequence is $0^+,2^+,4^+,6^+,\ldots$, in electron scattering experiments (where the initial state is inevitably the ground state), only transverse electric multipoles $F^{E\lambda}$ ($\lambda=2,4,\ldots$) can be measured for transitions within the ground-state band. (We will not discuss here contributions from longitudinal multipoles.) Accordingly, such experiments can provide information only on the $\mathcal{F}_R^{E\lambda}$ intrinsic multipoles, and not their magnetic counterparts $\mathcal{F}_R^{M\lambda}$.

Until now, the only experimental information on either $E\lambda$ or $M\lambda$ multipoles is that coming from static moments and γ transitions, from which "experimental" low-q values of $\mathcal{F}_R^{E\lambda}$, $\mathcal{F}_R^{M\lambda}$ can be obtained. In particular, (see Refs. 8 and 17)

$$\mathcal{F}_R^{E2}=\frac{1}{\sqrt{120}}\frac{q}{2\mathcal{I}}\frac{Q_0}{Z}\ , \tag{7}$$

$$\mathcal{F}_R^{M1}=-\sqrt{2/3}\frac{q}{2M}\frac{g_R}{Z}\ , \tag{8}$$

for $qR_0\ll 1$, where Q_0, $\mathcal{I}$, and g_R, are, respectively, the intrinsic quadrupole moment, the moment of inertia and the gyromagnetic ratio as defined in Ref. 21.

As mentioned in Sec. I, experimental information on the $E\lambda$ multipoles over an extended range of momentum transfers is expected[13] to be available in the near future from backwards (e,e') and coincidence $(e,e'\gamma)$ experiments. On the other hand, as pointed out in Ref. 15, the intrinsic $\mathcal{F}_R^{M\lambda}$ play a role in two related experimentally accessible transitions: (1) in odd-A nuclei where the magnetic form factors can be measured within the ground-state band, and (2) in collective $M1$ transitions to $K^\pi=1^+$ bands which have recently been observed in even-even rare-earth nuclei.[5,22] This renders our analysis of the succeeding sections, which covers a wide range of q values, interesting for future comparison to experimental data.

For the numerical calculations presented in this paper we used HF+BCS wave functions of the Sk-3 (Ref. 23) and Ska (Ref. 24) interactions, with occupation numbers determined by solution of the BCS equations in the constant-gap Δ mode. The single-particle states are eigenfunctions of the axially symmetric HF Hamiltonians obtained with different density dependent effective interactions. To further illuminate our discussion we employ also Nilsson single-particle states. In the HF case, the basis states are selected from ten major shells of the axially symmetric oscillator well in cylindrical coordinates,[8,25] while in the Nilsson case the states are defined on a basis of seven major spherical shells. In either case, the explicit expressions employed for the $\mathcal{F}_R^{\sigma\lambda}$ can be found in Ref. 17. Further details of the computational procedures can be found in Refs. 8 and 26.

Also included in the next section are results of the rigid rotor (RR) and irrotational fluid flow (IF) models. The results shown correspond to the simplest possible assumption of coincident uniform mass and charge distributions with quadrupole deformation. Under this assumption, to lowest order in the deformation parameter β, the intrinsic multipoles in the IF and RR models are given by[11–17]

$$(\mathcal{F}_R^{M1})_{\rm IF}=-\sqrt{6}\frac{j_1(qR_0)}{2AMR_0}\ , \tag{9a}$$

$$(\mathcal{F}_R^{M1})_{\rm RR}=\frac{-\sqrt{6}}{2AMR_0}[j_1(qR_0)+j_3(qR_0)(1+\sqrt{5/16\pi}\beta)^{-1}]\ , \tag{9b}$$

$$(\mathcal{F}_R^{E2})_{\rm IF}=\sqrt{2\pi/3}\frac{j_1(qR_0)+j_3(qR_0)}{5AMR_0\beta}\ , \tag{10a}$$

$$(\mathcal{F}_R^{E2})_{\rm RR}=\sqrt{3/2\pi}\frac{3\beta}{8AMR_0}[j_1(qR_0)-\tfrac{2}{3}j_3(qR_0)]\times(1+\sqrt{5/16\pi}\beta)^{-1}\ , \tag{10b}$$

$$(\mathcal{F}_R^{M3})_{\rm IF}=\sqrt{8/7}\frac{j_3(qR_0)}{2AMR_0}\ , \tag{11a}$$

$$(\mathcal{F}_R^{M3})_{\rm RR}=\sqrt{8/7}\beta\tfrac{3}{2}\sqrt{5/\pi}\frac{j_3(qR_0)}{2AMR_0}(1+\sqrt{5/16\pi}\beta)^{-1}\ , \tag{11b}$$

where β is the deformation parameter as defined in Ref. 21, and we have used the fact that under the assumption previously mentioned one has $g_R=Z/A$, $Q_0=3Z/\sqrt{5\pi}R_0^2\beta$, $\mathcal{I}_{\rm IF}=9AM(R_0\beta)^2/(8\pi)$,

$$\mathcal{I}_{\rm RR}=\tfrac{2}{5}AMR_0^2(1+\sqrt{5/16\pi}\beta)\ . \tag{12}$$

III. CALCULATIONS

A. Overview

As discussed in Sec. I the main purpose of this paper is to analyze the predictions of various rotational models (PHF, cranking, RR, and IF) for collective transverse form factors. In the case of microscopic models, the results depend not only on the model considered for a description of the rotational band (PHF or cranking), but also on the interaction used to determine the mean field, and on the basis of states employed to express the wave functions. In this paper we have used two Skyrme-type interactions, Sk-3 and Ska. The main reason for using Sk-3 is that we have a stock of self-consistent fields for it. Other virtues one can cite are that it provides a good fit to masses,[23] and has a good effective mass m^*/m.[27] It has been extensively used in computations for deformed nuclei and provides good deformation properties.[3,28] However, Sk-3 has too high a modulus of compressibility, underestimates the central charge density,[29] and overestimates the charge mean-square radii.[23] The Ska force of Köhler corrects in part for these deficiencies while maintaining other good features of Sk-3.[24–29]

We begin this section by discussing the problem of convergence of the numerical results with increasing size of the basis. This is done in Sec. III B where, to simplify matters, we present results only for ^{166}Er obtained with the Sk-3 interaction. The effect of using different effective interactions is explored in Sec. III C, where we devote our attention to disentangling orbital and spin contributions to the $M1$, $E2$, . . . multipoles. We discuss results for ^{166}Er, ^{156}Gd, and ^{174}Yb obtained in the cranking model with the Sk-3 and Ska forces, as well as with Nilsson model wave functions. For comparison we present some results obtained in the PHF model with the Sk-3 interaction. Finally, in Sec. III D we compare the PHF and cranking model results obtained with the Sk-3 interaction to those of the RR and IF models for several even rare-earth nuclei. The predictions at low q are also discussed and compared to "experimental" values deduced from Eqs. (7) and (8) of Sec. II. In all the figures it is the absolute value of the multipole which is plotted, but the sign of each peak is noted adjacently.

B. Convergence questions

In this section we discuss the accuracy of the numerical results. Our form factor calculations were done by adapting the code used for PHF calculations in Ref. 8. Modifications were made to include the cranking results, and to accept as input the wave functions computed with the McMaster version of the deformed HF code.[30]

The general form of the matrix elements entering into the form factors in the PHF and cranking models (see Ref. 17 and references therein for details) is

$$S_p^T=\sum_{\alpha,\beta}(u_\alpha v_\beta-v_\alpha u_\beta)^2(E_\alpha+E_\beta)^p\times\langle\alpha\,|\,j_+\,|\,\beta\rangle\langle\alpha\,|\,T_+\,|\,\beta\rangle\ , \tag{13}$$

where α,β label the HF single-particle states; E_α are quasiparticle energies; T_+ stands for any of the multipole or j_+ operators and p takes the values $0,-1$ in the PHF and cranking models, respectively. Since both occupied and empty levels contribute to Eq. (13), the results may be very sensitive to the size of the basis employed. This sensitivity is reduced in the case of the cranking model by the presence of the energy denominator, ($p=-1$), which provides a natural convergence factor, but it remains for the PHF case. However, when $p=0$, we may use closure to rewrite Eq. (13) in a form which effectively uses a complete basis:

$$S_{p=0}^T=\sum_\alpha v_\alpha^2\langle\alpha\,|\,T_+j_-+T_-j_+\,|\,\alpha\rangle-2\sum_{\alpha,\beta}v_\alpha v_\beta(v_\alpha v_\beta+u_\alpha u_\beta)\langle\alpha\,|\,j_+\,|\,\beta\rangle\langle\alpha\,|\,T_+\,|\,\beta\rangle\ . \tag{14}$$

In what follows we shall refer to Eqs. (13) and (14) as the "two-body" and "two-body+one-body" formulae for the $p=0$ case. Since Eq. (14) involves only occupied states, it will give better accuracy than Eq. (13) for the PHF case.

On the other hand, when doing both PHF and cranking calculations, it is much more convenient to use only one formulation, and because there is no equivalent to Eq. (14) for the $p=-1$ case, we are obliged to use the "two-body" formula for both models for economy of coding. In addition, it is much faster to use Eq. (13).

The accuracy of this procedure can be gauged by a

TABLE I. Cranking moment of inertia and $\langle J_\perp^2 \rangle$ values for neutrons and protons in ^{166}Er obtained with Sk-3 for different $E_{\rm cut}$ values. The $\langle J_\perp^2 \rangle$ without (with) parentheses correspond to results with the "two-body+one-body" ("two-body") method.

$E_{\rm cut}$ (MeV)	$\mathcal{J}_{\rm cr}^p$ (MeV^{-1})	$\mathcal{J}_{\rm cr}^n$ (MeV^{-1})	$\langle J_\perp^2 \rangle_p$	$\langle J_\perp^2 \rangle_n$
10			56.15	84.18
	10.18	18.21	(51.74)	(80.66)
30			56.15	84.15
	10.35	18.34	(55.52)	(83.62)
"Complete"			56.15	84.15
basis	10.35	18.34	(55.94)	(83.95)

comparison of the results of the two formulae as applied to the PHF model. In Table I we show values obtained for $\langle J_\perp^2 \rangle$ in the two cases, as well as for $\mathcal{J}_{\rm cr}$ using Eq. (13). The Sk-3 interaction was used. The parameter $E_{\rm cut}$ is one which truncates the basis states in the HF code; higher values retain more states from the ten major shells of the deformed oscillator basis. The last row corresponds to including all states from the ten major shells, while the second and third rows correspond to bases comprising all HF s.p. states with $E \leq E_{\rm cut}$, for the indicated values of $E_{\rm cut}$.

The expected trends of convergence evident in this table are as follows. (a) Using the two-body formula, convergence is faster for $\mathcal{J}_{\rm cr}$ than for $\langle J_\perp^2 \rangle$. (b) For $\langle J_\perp^2 \rangle$ convergence is faster using the "two-body+one-body" method.

A similar analysis was carried out for the form factors. Since these depend on momentum transfer, varying phases ensure that the accuracy can be no higher than for the examples given above. Nevertheless, we found that using the "two-body" method with $E_{\rm cut}=30$ MeV good accuracy was attained for the dominant contributions to the various $M1$, $E2$, $M3$, $E4$, and $M5$ multipoles. For these multipoles and in the least favorable case of the PHF model, the error in the dominant contribution is less than 5% when $E_{\rm cut}=30$ MeV. For $E6$, the situation is not as good. All this is illustrated in Fig. 1, where we show the main peaks of the proton convection [Fig. 1(a)] and magnetization [Fig. 1(b)] contributions to the different $M1$–$E6$ intrinsic multipoles in ^{166}Er (Sk-3 interaction). The "two-body" method for $E_{\rm cut}=10$ MeV (dashes) and 30 MeV (dots) is compared to the "exact" results of the "two-body+one-body" method. For the purpose of this discussion, the centre of mass and finite nucleon size effects, which do not affect convergence, have been omitted. As can be seen in the figure, for $M1$ convergence is already attained at $E_{\rm cut}=10$, while for the higher multipoles $E_{\rm cut}=30$ MeV is required. Although it is not fully seen in this figure, the convection contributions to the $M1$ and $E2$ multipoles dominate over the total magnetization contributions in the small momentum transfer region $q \leq 1.15$ fm^{-1}, while at larger momentum transfers the situation is reversed. This is discussed in more detail in the next section, along with the effect on the form factors of using different effective interactions. The trend observed in Fig. 1, in which the contributions are plotted only in the q regions where the main peaks appear, is observed over the entire momentum transfer region; i.e., within each multipole, convergence is attained faster for the dominant contribution. For example, on the left-hand side of Fig. 1(a), the larger $M1$ peak is converged at $E_{\rm cut}=10$ MeV while the smaller $E2$ peak requires 30 MeV. It is also evident in the figure that, except for $E6$, very good accuracy is attained in all multipoles with the "two-body" method, for $E_{\rm cut}=30$ MeV. Accordingly, all further results in this paper correspond to this value for $E_{\rm cut}$.

C. Intrinsic multipoles: Dependence on the Interaction

In this section we compare numerical results obtained using the Nilsson model and the effective interactions Sk-3 and Ska for the nuclei ^{156}Gd, ^{166}Er, and ^{174}Yb. For the latter two nuclei the Sk-3 mean fields are the same as in Ref. 3 where the collective gyromagnetic ratio and moment of inertia were calculated. For ^{156}Gd, the mean field was obtained by iterating from the field for ^{158}Gd. For the Ska interaction, the fields were obtained by iterating from the corresponding Sk-3 self-consistent fields. Pairing correlations were included by solving the BCS equations in the fixed gap mode.[25] Twenty iterations were sufficient to obtain good convergence.

The mean fields for the Sk-3 and Ska interactions differ in several ways: Their spatial extent, their shape (deformation), and in the pairing occupations (v_α^2). These differences were limited by specifying the same pairing gap and by using the same deformed harmonic oscillator basis (i.e., $b_\perp, b_z$) for the two forces, rather than searching for a new optimal basis. The effective mass is different for each of the three models: $m^*/m=1.0$ (Nilsson), 0.77 (Sk-3), 0.61 (Ska), and this has an effect on the occupation numbers by altering the level density at the Fermi surface. A particularly important source of difference between the Nilsson model and the other results is in the

TABLE II. Field and pairing parameters of the Nilsson calculation.

	b (fm)	δ	Δ_p (MeV)	Δ_n (Mev)
^{156}Gd	2.10	0.279	0.963	1.07
^{166}Er	2.14	0.277	0.915	0.903

single-particle wave functions, which in the Nilsson model contain much less high n,l,j components. This implies that the multipoles will be located more to the outside in coordinate space, and that they will fall off more rapidly with momentum for the Skyrme forces. The parameters adopted for the Nilsson model calculations are shown in Table II. (The χ and μ values are chosen as in Ref. 31.) Table III contains the proton and neutron pairing gaps used in the HF calculations, as well as the results for binding energy, charge radius, quadrupole Q_2, and hexadecupole Q_4 moments obtained using the Sk-3 (Ska in parentheses) force. As can be seen in the table, the charge radii differ by less than 1% between the two forces, while the Q_2 and Q_4 moments differ somewhat more (but ≤ 4 and 10%, respectively). While the Q_2 moments are of the same order of magnitude for all nuclei considered, the Q_4 moments vary by a factor of 10 in going from ^{154}Sm to ^{174}Yb. This, as will be discussed below,

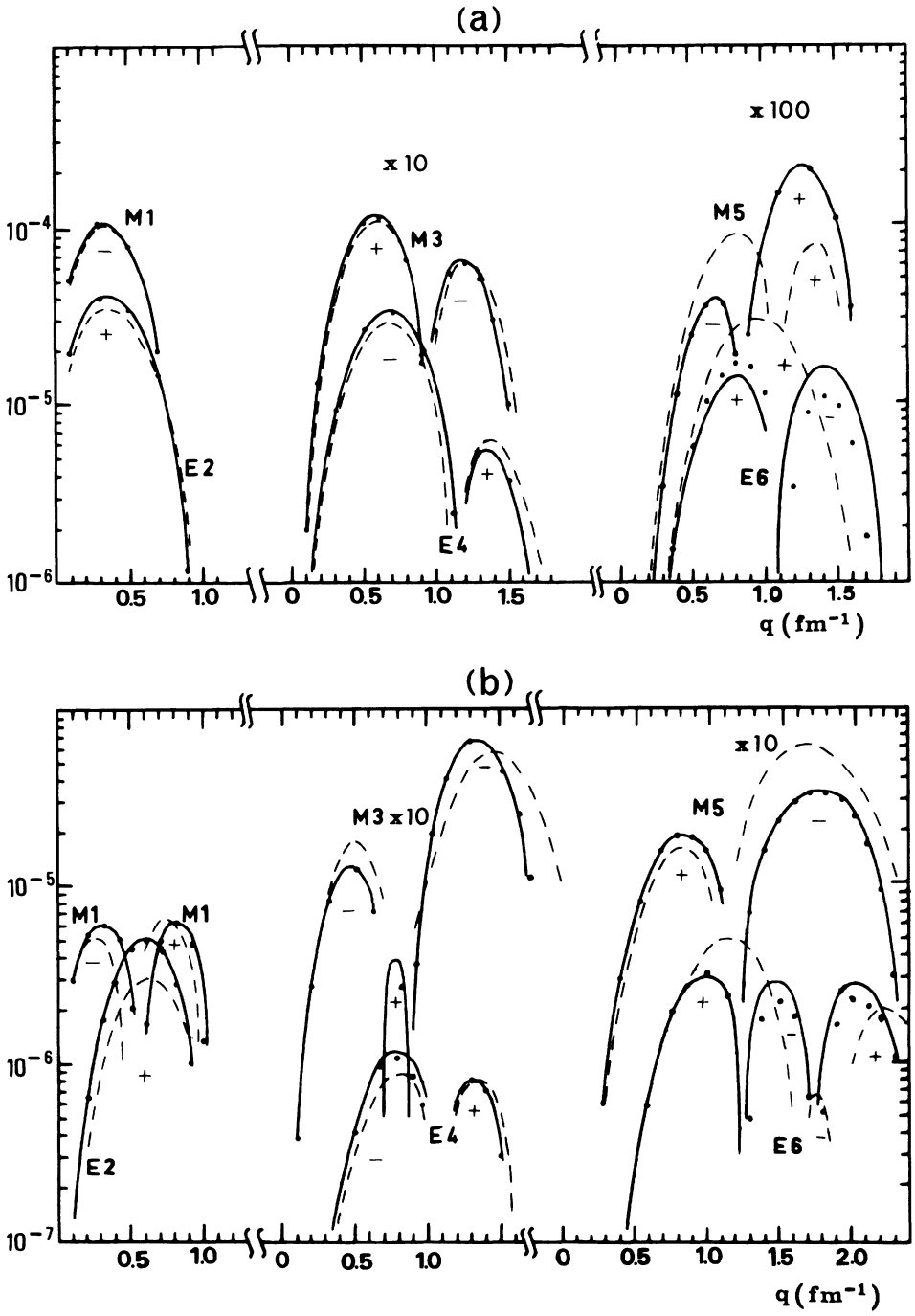

FIG. 1. Proton convection (a) and magnetization (b) contributions to $M1$–$E6$ multipoles for ^{166}Er with PHF model (Sk-3 force). Results obtained with the "two-body" method for $E_{\text{cut}}=10$ (— — —) and $E_{\text{cut}}=30$ (· · ·) are compared to the "exact" results of the "two-body + one-body" method (——).

has important effects on the $M3$ and $E4$ form factors. All results shown in this and the next section contain the centre of mass (c.m.) and finite nucleon size (NFS) corrections. For the c.m. correction the usual factor

$$f_{\text{c.m.}}(q)=e^{b^2q^2/4A} \tag{15}$$

was included, with $b=A^{1/6}$ fm. For the nucleon magnetic form factors we used the dipole expression

$$G_\tau^M(q)=\mu_\tau(1+q^2/18.23\ \text{fm}^2)^2\ , \tag{16}$$

while for the proton electric form factor we used the sum of monopoles fitted by the Mainz group:[32]

$$G_p^E(q)=\sum_n a_n/(1+q^2/m_n^2)\ , \tag{17}$$

where the parameters take the values

$$m_1^2=6.0,\quad m_2^2=15.02\ ,$$

$$m_3^2=44.08,\quad m_4^2=154.2\ \text{fm}^2\ ,$$

$$a_1=0.312,\quad a_2=1.312\ ,$$

$$a_3=-0.709,\quad a_4=0.085\ .$$

For the neutron electric form factor we took the difference of two Gaussians:

$$G_n^E(q)=\exp(-q^2r_+^2/4)-\exp(-q^2r_-^2/4) \tag{18}$$

with[33] $r_\pm^2=0.5074\mp0.038664$ fm^2. (This gives $r_n^2=-0.1160$ fm^2.) In the numerical calculations, first the convection (c) and the magnetization (m) contributions from point Dirac nucleons ($g_n=g_p=1$) to the intrinsic multipoles $[\mathcal{T}_R^{\sigma\lambda}(q)]_{\tau=p,n}^{\rho=c,m}$ are computed. They are then multiplied by the c.m. factor and the appropriate nucleon form factors to give

$$[\mathcal{T}_R^{\sigma\lambda}(q)]_{pc}=[\mathcal{T}_R^{\sigma\lambda}(q)]_p^c G_p^E(q)f_{\text{c.m.}}(q)\ , \tag{19a}$$

$$[\mathcal{T}_R^{\sigma\lambda}(q)]_{nc}=[\mathcal{T}_R^{\sigma\lambda}(q)]_n^c G_n^E(q)f_{\text{c.m.}}(q)\ , \tag{19b}$$

$$[\mathcal{T}_R^{\sigma\lambda}(q)]_{pm}=[\mathcal{T}_R^{\sigma\lambda}(q)]_p^m G_p^M(q)f_{\text{c.m.}}(q)\ , \tag{19c}$$

$$[\mathcal{T}_R^{\sigma\lambda}(q)]_{nm}=[\mathcal{T}_R^{\sigma\lambda}(q)]_n^m G_n^M(q)f_{\text{c.m.}}(q)\ . \tag{19d}$$

Finally, the intrinsic multipoles are found by summing the four contributions in Eq. (19). It is these intrinsic multipoles which are shown in the cases $\lambda=1,3$; while for $\lambda=2,4$, unless specified otherwise, the results shown correspond to the transition multipoles [see Eq. (1)]

$$F^{E\lambda}(q)=\lambda(\lambda+1)\mathcal{T}_R^{E_\lambda}(q),\quad \lambda=2,4\ . \tag{20}$$

We now analyze the dependence of the individual $[\mathcal{T}_R^{\sigma\lambda}(q)]_{\tau\rho}$ contributions on the force, taking ^{166}Er as an example. We shall see in detail which contributions are most sensitive to varying the mean field or the rotational model. We shall also see which contributions dominate in different regions for each multipolarity. In Figs. 2–5 we show the results obtained for $[\mathcal{T}_R^{M1}(q)]_{\tau\rho}$, $[\mathcal{T}_R^{E2}(q)]_{\tau\rho}$, $[\mathcal{T}_R^{M3}(q)]_{\tau\rho}$, and $[\mathcal{T}_R^{E4}(q)]_{\tau\rho}$, respectively, for ^{166}Er. Each figure is organized so that the individual (τ,ρ) contributions appear separately. Parts (a), (b), (c), and (d) correspond to those given in Eqs. (19a)–(19d). The lines are coded as follows: Cranking model using the Nilsson (dash-dot), Ska (dotted), Sk-3 (dashed) forces, and PHF model using the Sk-3 force only (solid line). The total $M1$–$E4$ multipoles for ^{166}Er are shown in Fig. 6.

In Fig. 2 ($M1$) one can see that strong cancellations occur between the proton and neutron magnetization contributions in the low q region up to about 1.5 fm^{-1}, while the convection contributions add coherently. But because the neutron charge is zero, the convection term comes almost entirely from the protons. In the higher q region, $q>1.5$ fm^{-1}, constructive interference occurs between pm and nm contributions, and magnetization dominates over convection. These general features are repeated for the different models and forces, as well as for the different nuclei considered in this paper. The difference in results between the Ska and Sk-3 forces is visible only in the pm and nm contributions and is inappreciable when the total $\mathcal{T}_R^{M1}$ multipole is plotted. Larger changes are however observed in all the individual contributions when Nilsson model wave functions are used. When one compares the Sk-3 and Nilsson results in Fig. 2, the main difference is that the peaks are broader and shifted to higher q for the Nilsson model. As mentioned earlier, this is because the Nilsson wave functions have a larger

TABLE III. Gap parameters for protons and neutrons used in the HF calculations and results for binding energies; charge radii proton and neutron rms radii; quadrupole and hexadecupole moments. Values within parentheses correspond to the results with the Ska effective interaction.

	Δ (MeV)		B (MeV)	$\langle r^2\rangle^{1/2}$ (fm)			Q_2 (fm^2)		Q_4(10^5 fm^4)	
	p	n		c	p	n	p	n	p	n
^{154}Sm	1.120	1.20_0	1257.33	5.17_0	5.130	5.227	651.7	922.6	0.115	0.175
^{156}Gd	0.904	0.881	1270.38	5.20_5	5.164	5.243	693.1	943.5	0.115	0.174
			(1269.60)	(5.15_5)	(5.111)	(5.261)	(692.2)	(952.6)	(0.110)	(0.175)
^{158}Gd	0.904	0.881	1284.51	5.22_5	5.184	5.274	721.5	1015.0	0.114	0.176
^{164}Dy	0.952	0.872	1326.12	5.28_5	5.247	5.342	771.3	1114.0	0.086_5	0.134
^{166}Er	0.916	0.903	1338.96	5.31_5	5.275	5.355	788.4	1106.0	0.076	0.120
			(1338.72)	(5.26_5)	(5.224)	(5.376)	(795.0)	(1126.0)	(0.068)	(0.113)
^{168}Er	0.916	0.903	1353.33	5.33_0	5.291	5.382	799.7	1152.0	0.062_7	0.099_7
^{174}Yb	0.831	0.682	1393.46	5.37_5	5.337	5.434	782.5	1147.0	0.0112	0.0234
			(1394.47)	(5.33_0)	(5.288)	(5.461)	(804.3)	(1185.0)	(0.0117)	(0.0234)

content of low nlj components as compared to those of the HF calculations. Also the strength of the peaks is somewhat larger for the Nilsson model results (particularly so for the magnetization contributions). This occurs because the cranking moment of inertia is smaller when calculated from the Nilsson model wave functions (see Table IV). On the other hand, comparing the results in Fig. 2 of the PHF and cranking models (Sk-3 force), one sees that the dominant peak of the proton convection contribution does not change much, but the strength of the magnetization contribution is substantially lower in the PHF model. Hence, the total $\mathcal{T}_R^{M1}$ multipole (see Fig. 6) obtained in the PHF model differs more from that of the cranking model (with the same interaction) in the higher q region (>1.7 fm^{-1}). In Fig. 6 one sees that for the $M1$ multipole the differences caused by using Nilsson

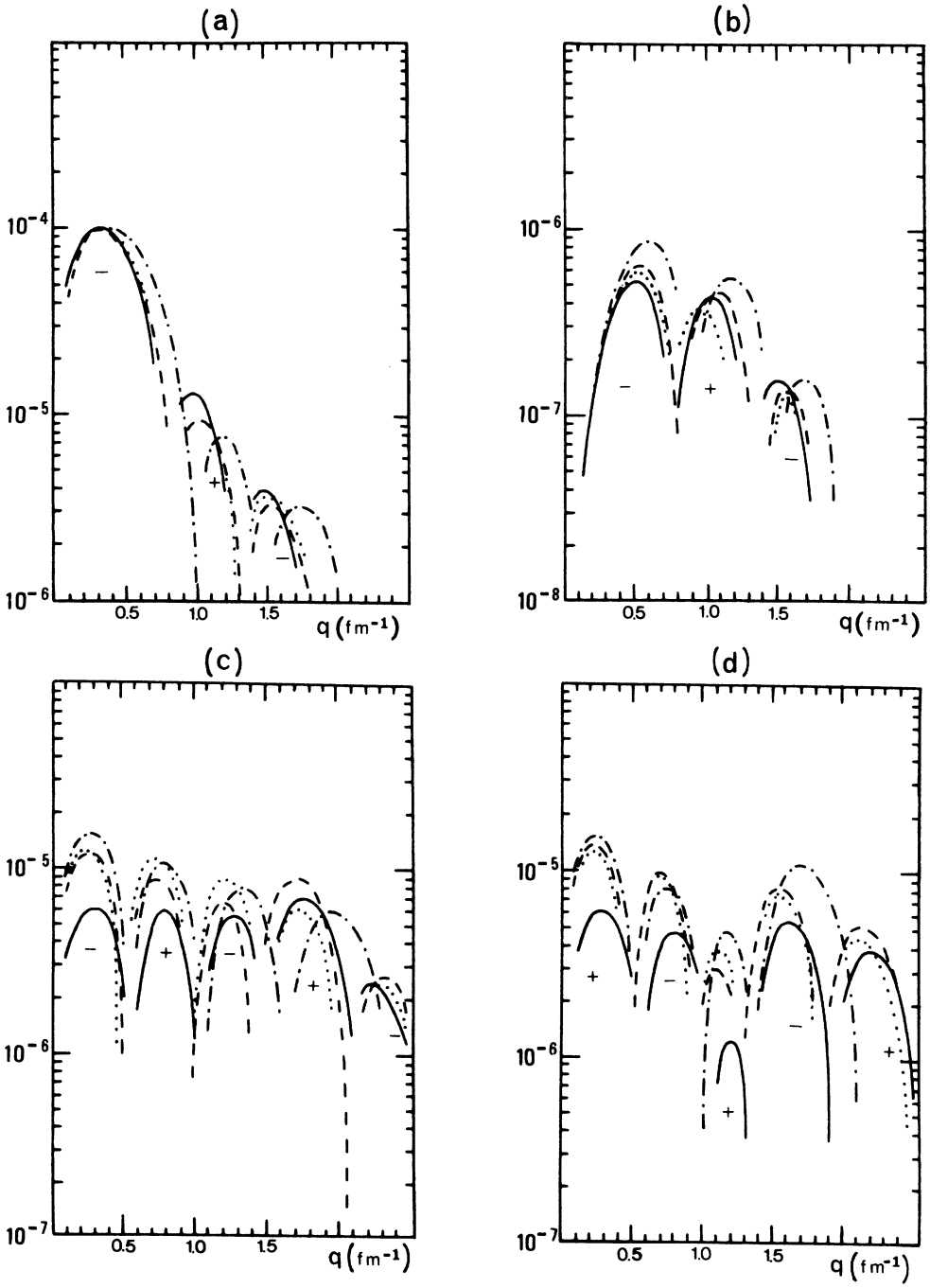

FIG. 2. Results of PHF model with Sk-3 (——) and cranking model with Sk-3 (— — —), Ska (· · ·), and Nilsson (—·—·—·) for the proton convection (a), neutron convection (b), proton magnetization (c), and neutron magnetization (d) contributions to the intrinsic $M1$ multipole in ^{166}Er.

model as opposed to HF wave functions are more important than those caused by using the PHF as opposed to the cranking model. This situation is practically reversed when one considers the $E2$ multipole; see Fig. 6.

The individual $[\mathcal{T}_R^{E2}]_{\tau\rho}$ contributions are shown in Fig. 3. Here one can see that the $E2$ contributions depend more strongly on both the mean field and on the rotational model than in the case of the $M1$ multipole. In particular, the strength of the first peak in the convection current contribution at $q \sim 0.3$ fm^{-1} decreases by a factor of 3 in going from PHF to the cranking model. As in the $M1$ case, the magnetization contributions for protons and neutrons interfere destructively in the low q region ~ 1 fm^{-1}, where the dominant contribution is the proton convection current, while again at $q \geq 1.5$ fm^{-1} the magnetization contribution dominates. Also, although differences between Sk-3 and Ska results are larger than in the $M1$ case, they are closer to each other than they are to the Nilsson model results.

The main trends for the $E2$ form factor (see Fig. 6) are as follows. When one compares results obtained with HF or Nilsson models using a fixed rotational model, the

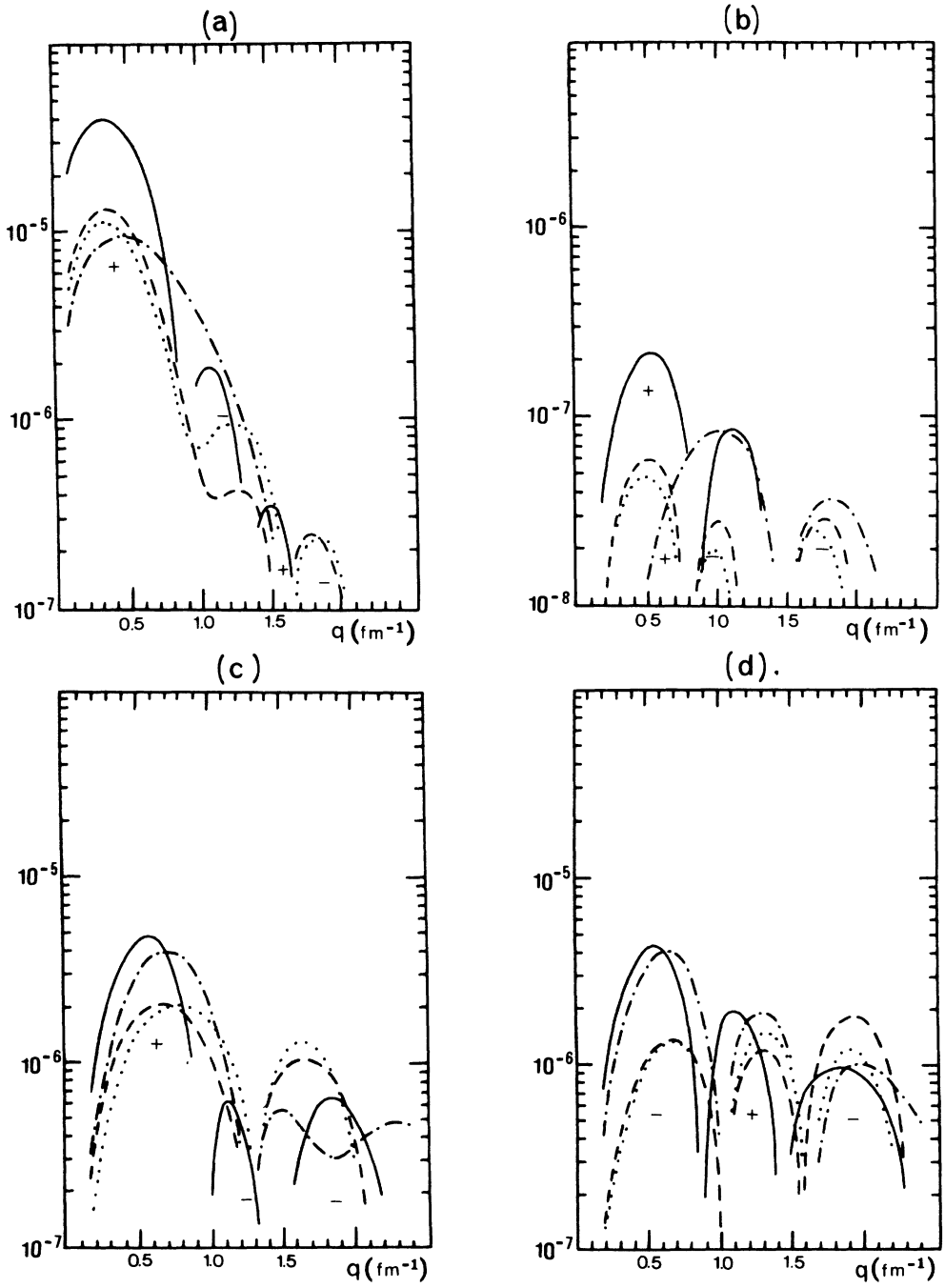

FIG. 3. Same as Fig. 2, for the intrinsic $E2$ multipole.

peaks are broader, slightly weaker, and shifted to larger q values, with the Nilsson model. This again reflects the broader spatial distribution of the HF currents. On the other hand, when one compares the PHF and cranking models results obtained with a fixed interaction, the strength of the first peak is strongly affected (roughly a factor of three) but its position is unchanged. In Ref. 12, nonperturbative cranking model calculations using a deformed Woods-Saxon potential were reported for ^{166}Er. Those results for the $E2$ form factor are in fair agreement with ours for the cranking model in first-order perturbation theory. As discussed in Ref. 26, the first $E2$ peak obtained by Wüst *et al.*[12] lies in between the cranking model results with Sk-3 and Nilsson shown in Fig. 6 in the whole low-q region ($q \lesssim 1.3$ fm^{-1}), and the strength and position of the peak is closer to the Sk-3 results. On the other hand, PHF results using the DME effective interaction for the $E2$ form factor in ^{166}Er were also reported in Refs. 8 and 11. Those results are similar to ours with the Ska interaction, which in turn are very close to those shown in Fig. 6 for Sk-3. The strength of the first peak with Ska and DME effective interactions is only 15%

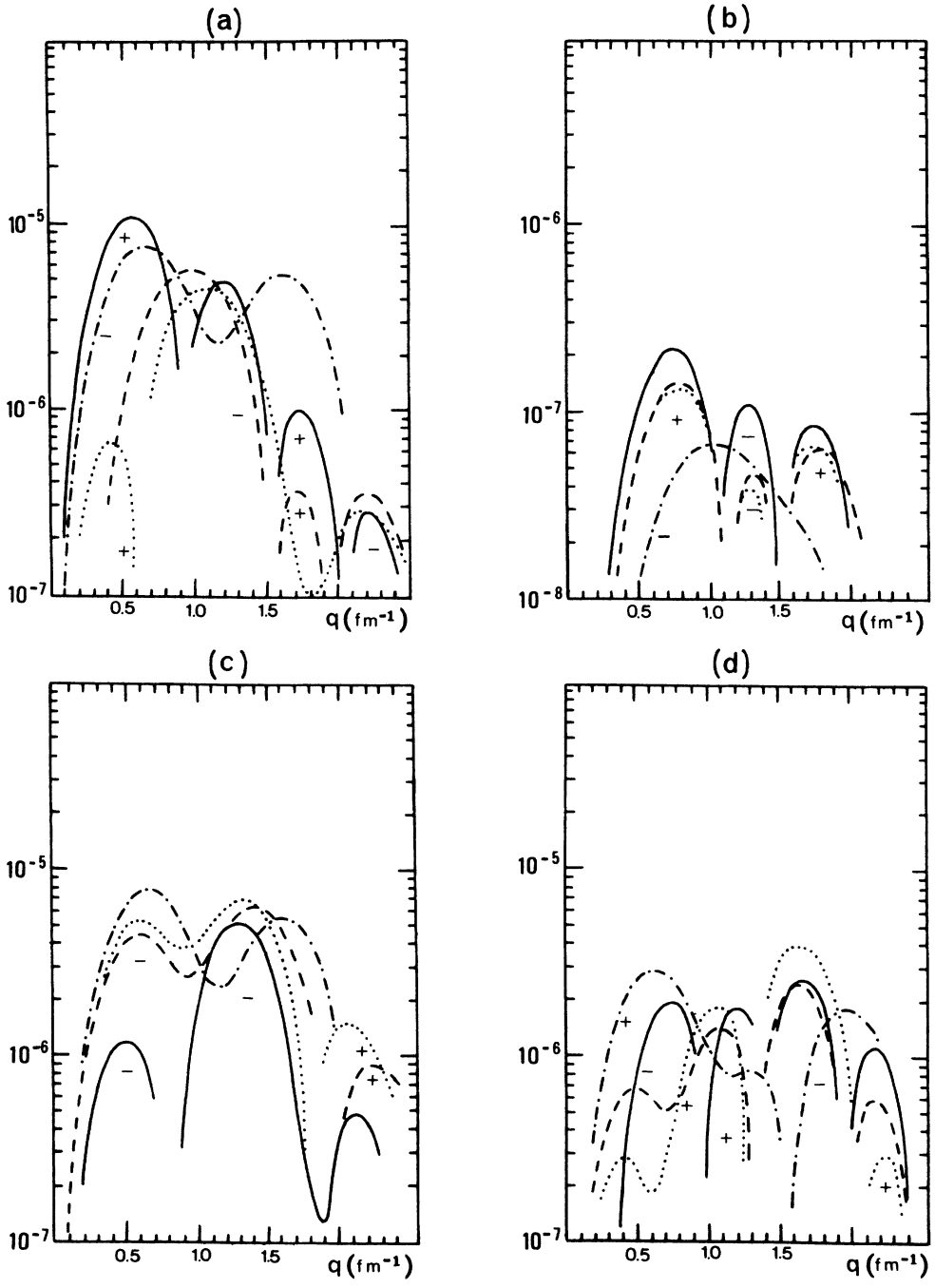

FIG. 4. Same as Fig. 2, for the intrinsic $M3$ multipole.

lower than with Sk-3. This similarity between Ska and DME results is expected on the basis of previous analyses of charge densities with various interactions.[10,24]

From Figs. 4 and 5 one sees that, as a general rule, with increasing multipolarity the sensitivity of the $[\mathcal{F}_R^{\sigma\lambda}]_{\tau\rho}$ contributions to the mean field is stronger. We also note that while Figs. 2 and 3 (for ^{166}Er) are representative of the general trends observed in the results obtained for the different nuclei, this is not the case for Figs. 4 and 5. This is to say, the individual $[\mathcal{F}_R^{\sigma\lambda}]_{\tau\rho}$ contributions for different nuclei change more with increasing multipolarity.

In particular in Fig. 4 one can see that the question of whether convection or magnetization contributions dominate in different q regions depends on which mean field and which rotational model one considers. For instance if we compare the results of PHF and cranking with the Sk-3 force, we see, in the neighborhood of $q \sim 0.5$ fm^{-1} (where convection and magnetization interfere destructively), that the convection contribution dominates in

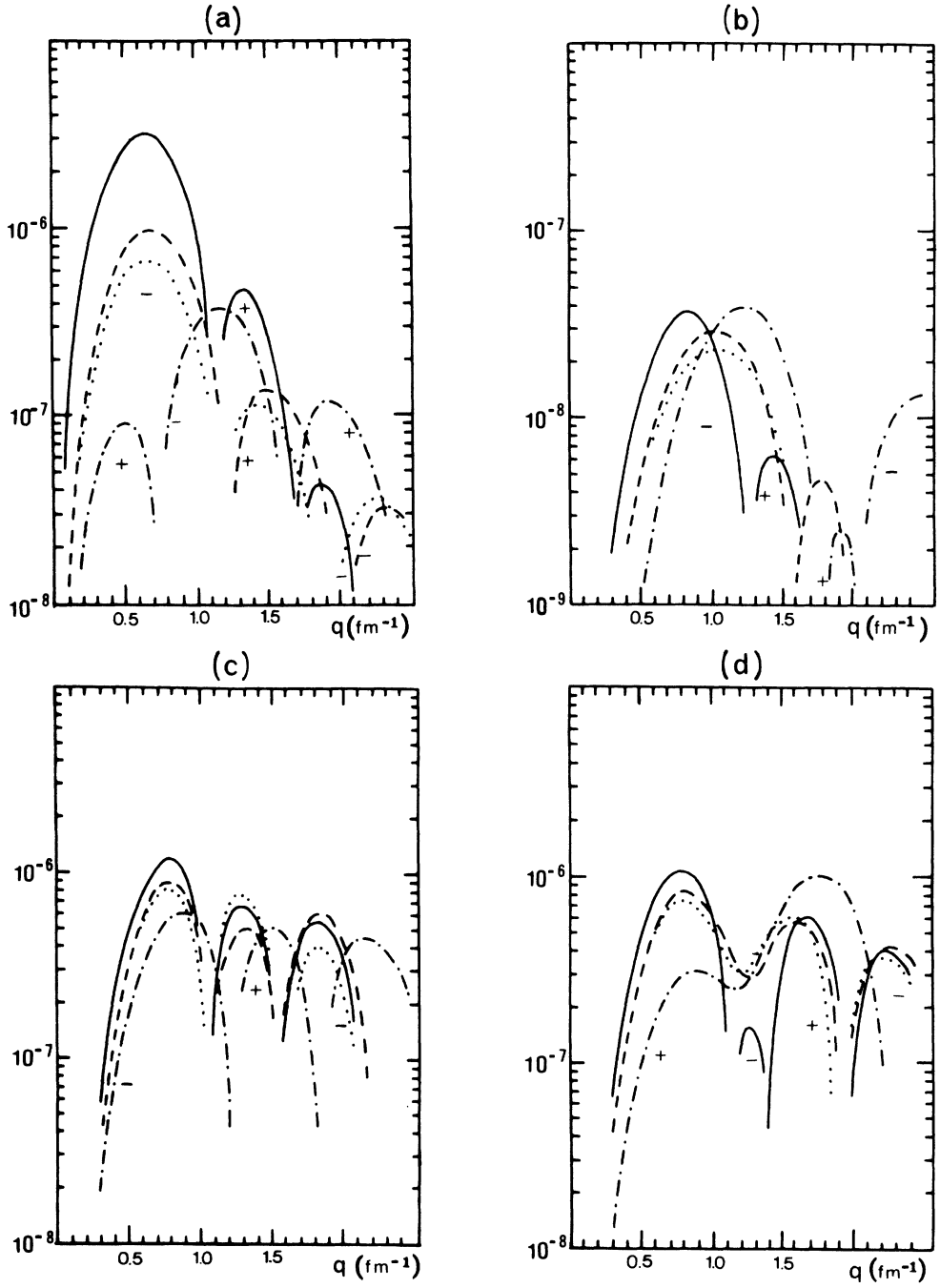

FIG. 5. Same as Fig. 2, for the intrinsic $E4$ multipole.

PHF and the magnetization contribution dominates in cranking. This results in a different phase at low-q between PHF and cranking results for the $M3$ multipole (see Fig. 6). In the neighborhood of $q \sim 1.4$ fm^{-1} convection and magnetization are comparable and add coherently in both PHF and cranking models. For $q > 1.7$ fm^{-1} magnetization dominates over convection. All this results in a more fragmented structure of the total $M3$ multipole (see Fig. 6) when using PHF. On the contrary, with the Nilsson model the $M3$ multipole is rather similar independently of whether PHF or cranking models are used.

For the $E4$ multipole one sees (Fig. 6) that the results of PHF and cranking models with a fixed mean field

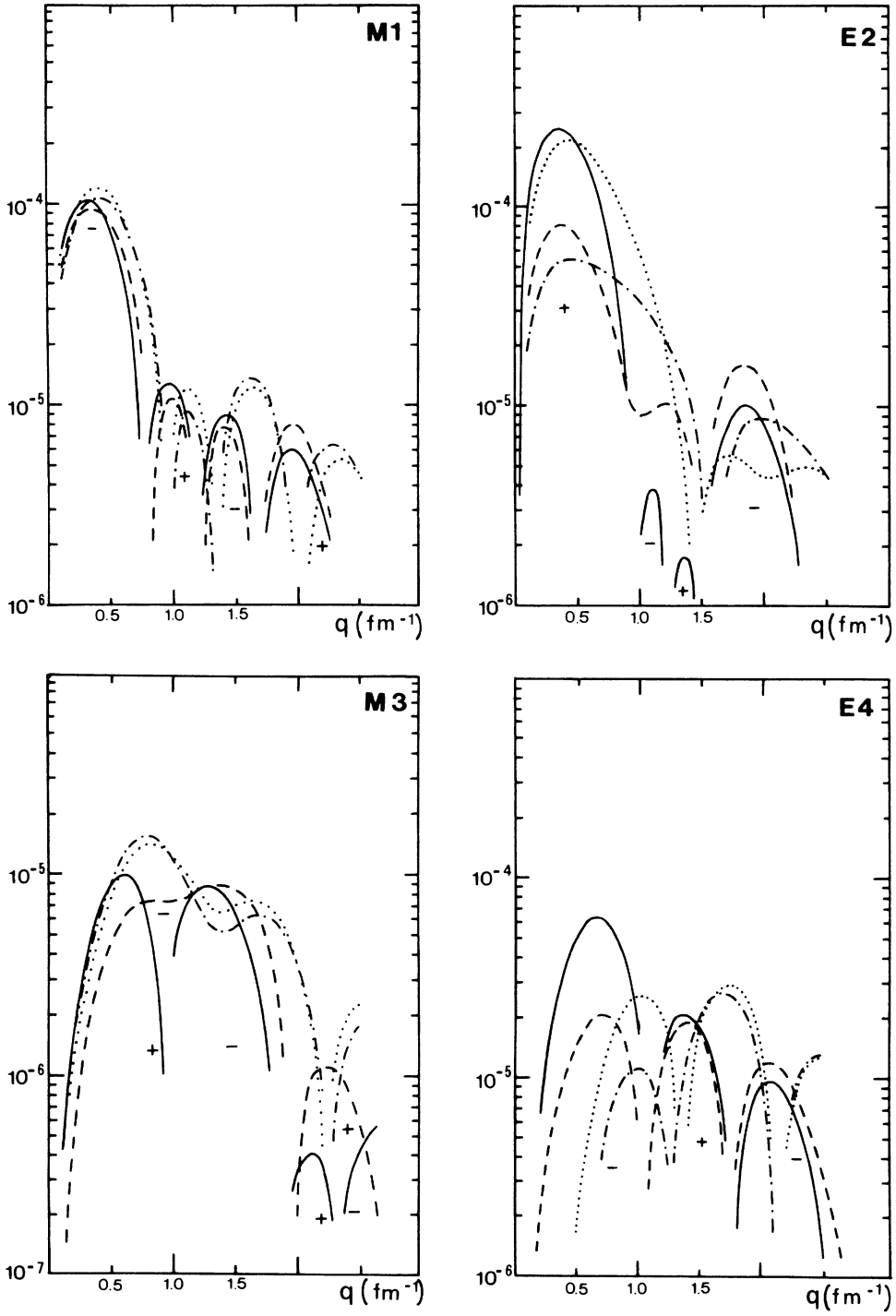

FIG. 6. Intrinsic $M1$, $M3$, and transition $E2$, $E4$ form factors of ^{166}Er in PHF model with Sk-3 (——) and Nilsson (· · ·) and in cranking model with Sk-3 (— — —) and Nilsson (—·—·—·) wave functions.

differ mainly in the strength of the main peak and the positions of the different peaks do not change. As in the case of the $E2$ multipole, the strength of the first $E4$ peak is of the order of a factor of 3 larger with PHF than with cranking. Note also (see Fig. 5) that convection dominates over magnetization for $q \lesssim 1.2$ fm^{-1}, the magnetization current dominates at $q \gtrsim 1.7$ fm^{-1} and in the transition region both are of comparable size. On the other hand with fixed rotational model, the results with HF or Nilsson wave functions differ both in the strength and position of the peaks. For instance using the PHF model the main peak of the $E4$ multipole with HF wave functions at $q \sim 0.7$ fm^{-1} is displaced to $q \sim 1.0$ fm^{-1} and its strength is reduced by a factor of 2 (the comparison is similar for the results of the cranking model). This difference is mainly due to the lower hexadecupole defor-

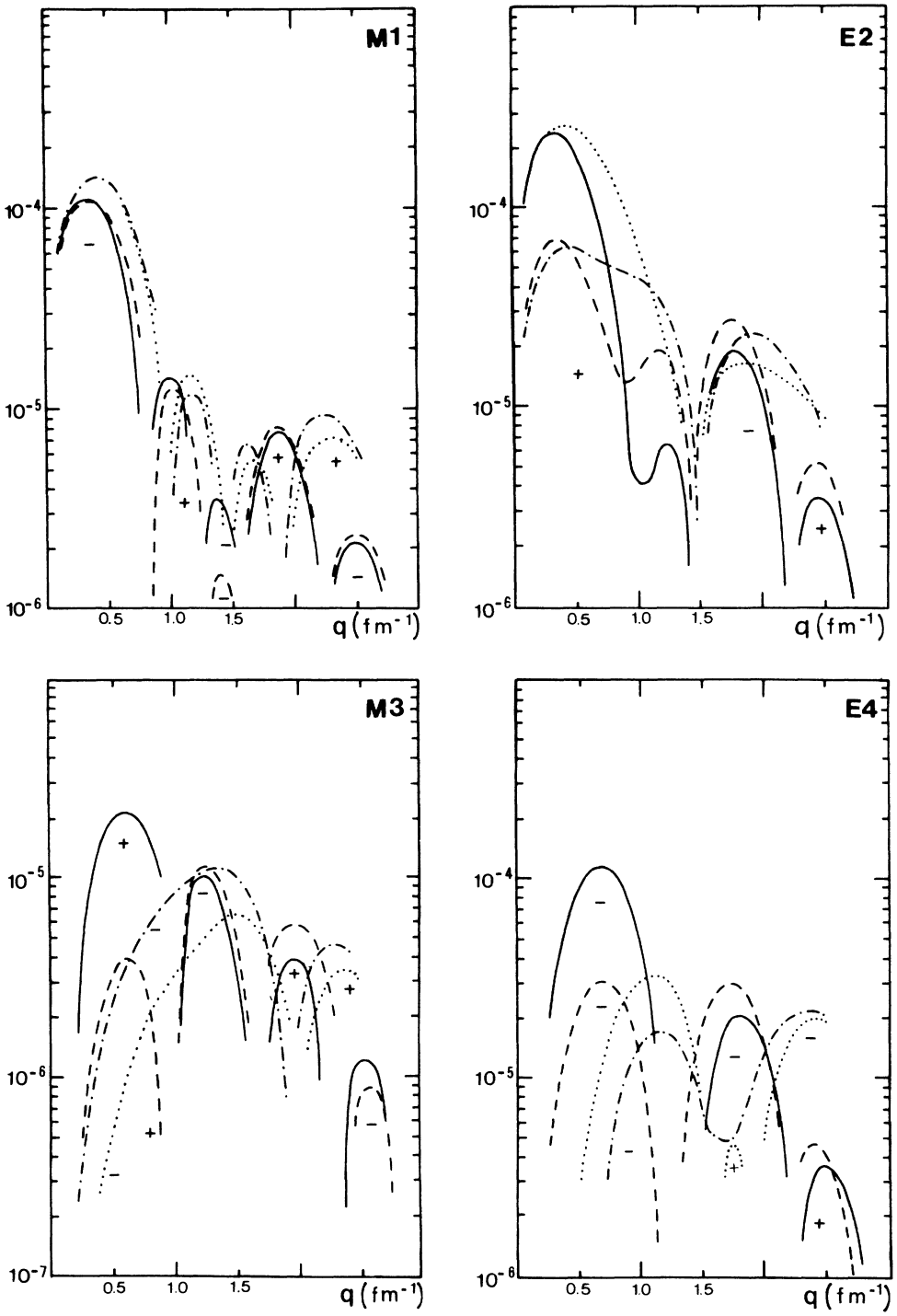

FIG. 7. Same as Fig. 6, for ^{156}Gd.

mation of the Nilsson densities, as can also be inferred from Fig. 5(a). This is also corroborated by inspection of the $E4$ results with the Sk-3 force for ^{166}Er, ^{156}Gd, and ^{174}Yb in Figs. 6, 7, and 8, respectively. Here one sees that the strength of the first $E4$ peak reduces in going from ^{156}Gd to ^{166}Er, and is strongly reduced and shifted to larger q value in ^{174}Yb. This is intimately connected with the reduction of the hexadecupole deformation observed in Table III.

In Figs. 6–8 one also sees that the results for $M1$ and $E2$ form factors are rather similar in the different nuclei, particularly as concerns the position and strength of their first peaks, which are dominated by the convection current. Since these features, strength and position of the

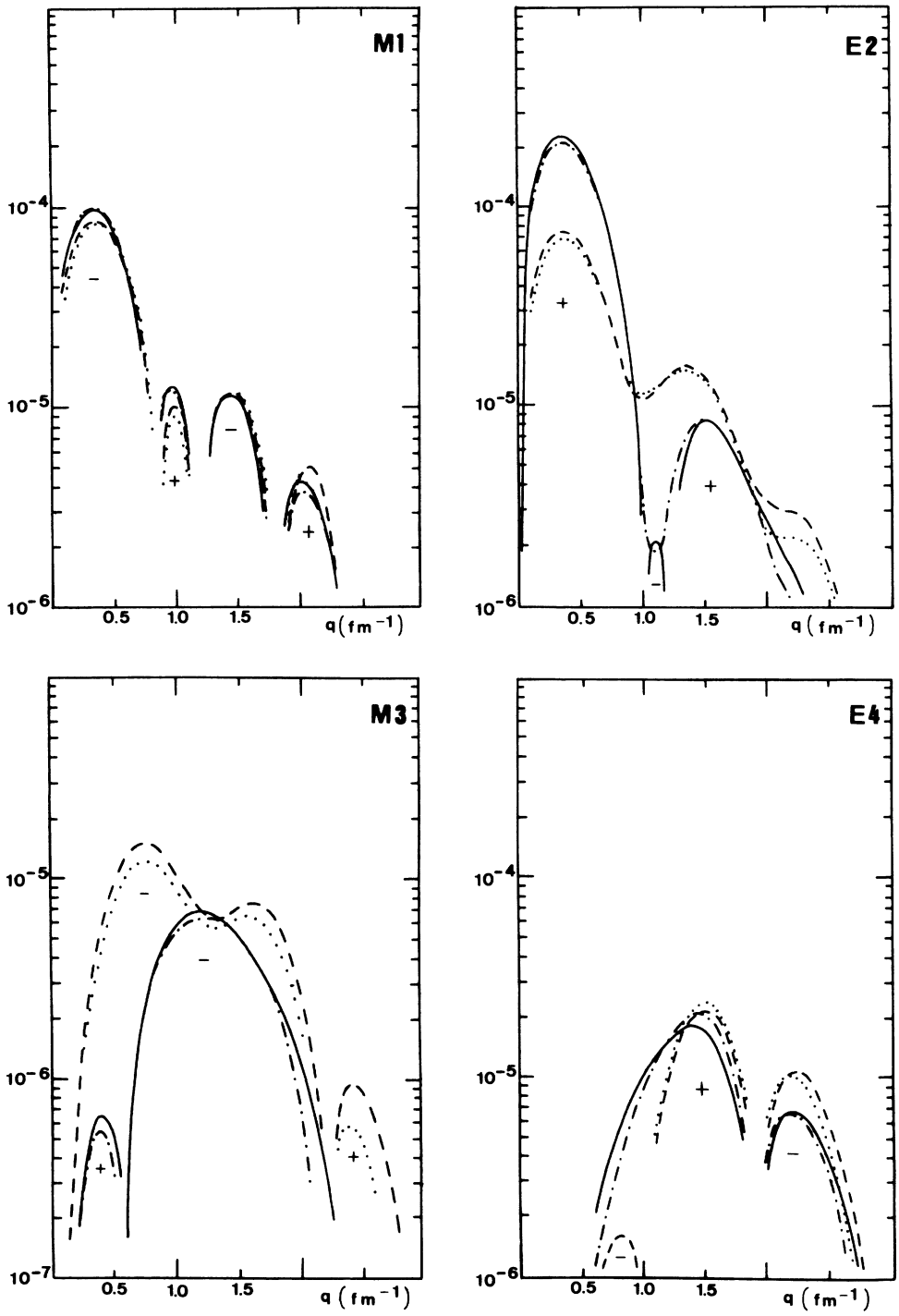

FIG. 8. Same as Fig. 6 for ^{174}Yb. In this case (· · ·) and (—·—·—·) correspond to results with Ska instead of Nilsson wave function.

first $M1$ and $E2$ peaks, do not change by more than 20% when Nilsson model instead of HF s.p. wave functions are used, the simpler Nilsson model can be used to get a reliable estimate of them. For the $M1$ multipole also the predictions of the PHF and cranking models are very close. This is consistent with the fact that the gyromagnetic ratios obtained with these two different rotational models are similar (see Table IV and Refs. 3 and 8). For the $E2$ multipole however the PHF model systematically predicts a strength of the first peak larger than the cranking model by a factor of 3. This can be related to the problem of current conservation which holds approximately[17] in the cranking model but not in PHF. Current conservation can be used to determine the $E2$ form factor at low q [see Eq. (7)]. We may then use this low-q value to scale the computed form factors. By doing that the first peak of the $E2$ multipole computed with PHF and cranking models would come very close, but at $q \gtrsim 0.8$ fm^{-1} the difference in the two model predictions would grow. This will be discussed in more detail in Sec. III D.

For the $M3$ multipole, as previously mentioned, the predictions of different models for various nuclei are quite distinct and no systematic behavior is apparent, except that the main strength seems to be spread in the region $0.5 \lesssim q \lesssim 2$ fm^{-1} and is of the same order for all cases. In particular we find with the Skyrme forces, a strong decrease of the convection contribution to this multipole, in going from ^{156}Gd and ^{166}Er to ^{174}Yb, that can be related to the decrease of the hexadecupole moment, which causes the completely different behavior observed at low $q < 0.6$ fm^{-1}.

For the $E4$ multipole, although predictions of different models for different nuclei also differ substantially, a more systematic behavior is found. The decrease of the $E4$ form factor in going from ^{156}Gd to ^{174}Yb (and in going from HF to Nilsson) can clearly be connected to the decrease of the hexadecupole deformation, as previously discussed. The systematic decrease of the first peak in going from PHF to cranking for each individual nucleus is connected to the same effect found in the $E2$ multipole form factor. Both connections can be traced back to the problem of current conservation (cc) which implies that at low q, the $E4$ form factor must be directly proportional to the hexadecupole moment Q_4 and inversely proportional to the moment of inertia $[1/\mathcal{I} = (\epsilon_{4+} - \epsilon_{0+})/10]$. This will be discussed in Sec. III D.

D. Comparison of microscopic and macroscopic models

We now compare the results of the PHF and cranking models to those of the rigid rotor (RR) and irrotational flow (IF) models, for several nuclei. For these macroscopic models, we use the simple approach sketched in Sec. II [see Eqs. (9a)–(11b)]. Then there is no $E4$ contribution and the RR and IF predictions change little from one nucleus to another as they involve only the parameters R_0 (which we choose as $R_0 = 1.12\ A^{1/3}$ fm) and β. Also, the $M3$ multipole has the same q dependence in the two models, which differ only by an overall factor of $1.7\beta \simeq 0.5$, RR being smaller. [See Eq. (11) and Figs. 9–12.]

The β value for each nucleus has been obtained from the quadrupole moment of its first excited 2^+ state:[34] $\beta = 0.28$ (^{154}Sm), 0.34 (^{156}Gd), 0.36 (^{158}Gd), 0.35 (^{164}Dy),

TABLE IV. Results obtained for $\mathcal{I}_{cr}$, gyromagnetic ratios (in PHF and cranking models) and $\langle J_1^2 \rangle$ with various fields. Experimental values for $\mathcal{I}$ and g_R are also shown.

		$\mathcal{I}$ (MeV^{-1})			g_R		$\langle J_1^2 \rangle$		
		Total	n	p	cr	PHF	Total	n	p
^{154}Sm	exp.	36.59			(0.29 to 0.40)				
	Sk-3	24.54	14.39	10.15	0.412_7	0.414_3	127.79	74.41	53.38
^{156}Gd	exp.	33.73			(0.2999 to 0.395)				
	Sk-3	31.11	19.51	11.60	0.351_1	0.400	140.78	83.37	57.41
	Ska	30.01	18.81	11.20	0.356_5	0.407	142.99	83.88	59.11
	Nilsson	20.88	12.00_2	8.88_1	0.425	0.445	88.90	49.35	39.55
^{158}Gd	exp.	37.73			(0.318 to 0.411)				
	Sk-3	29.88	18.22	11.66	0.376_1	0.401_5	144.51	85.52	58.99
^{164}Dy	exp.	40.88			(0.324 to 0.365)				
	Sk-3	30.27	19.18	11.09	0.344_9	0.387	144.49	87.28	57.21
^{166}Er	exp.	37.22			(0.303 to 0.333)				
	Sk-3	28.69_5	18.34_5	10.35	0.337_4	0.391	140.30	84.15	56.15
	Ska	28.90	18.09	10.81	0.355_6	0.405	144.90	85.33	59.57
	Nilsson	25.51	16.39	9.12	0.358	0.407	100.10	59.39	40.71
^{168}Er	exp.	37.59			(0.27 to 0.35)				
	Sk-3	28.12	18.01	10.11	0.347_4	0.389	142.67	86.29	56.38
^{174}Yb	exp.	39.22			(0.25 to 0.34)				
	Sk-3	31.13	20.71	10.42	0.306_2	0.377_5	145.27	89.00	56.27
	Ska	29.95	20.20	9.75	0.291_6	0.383_5	151.57	91.87	59.70

0.34 (^{166,168}Er), 0.35 (^{174}Yb). Because the PHF and cranking predictions for ^{156}Gd, ^{166}Er, and ^{174}Yb were already displayed in the previous section, we here show results for ^{154}Sm, ^{158}Gd, ^{164}Dy and ^{168}Er in Figs. 9–12, respectively. As in the preceding Figs. 6–8, the full and dashed lines correspond to PHF and cranking (Sk-3 force), respectively, while the dotted and dot-dashed lines correspond to the RR and IF models in that order.

The PHF and cranking model results follow the trends discussed in the previous section: (1) the $M1$ form factor with its main peak at $q \sim 0.3$ fm^{-1} is very similar in both models for all nuclei seen. (2) The $E2$, $M3$, and $E4$ multipoles are much more sensitive to the model used and to the particular structure of a given nucleus. (3) For the $E2$ multipole the main peak at $q \sim 0.3$ fm^{-1} is roughly three times larger in PHF than in cranking, while for

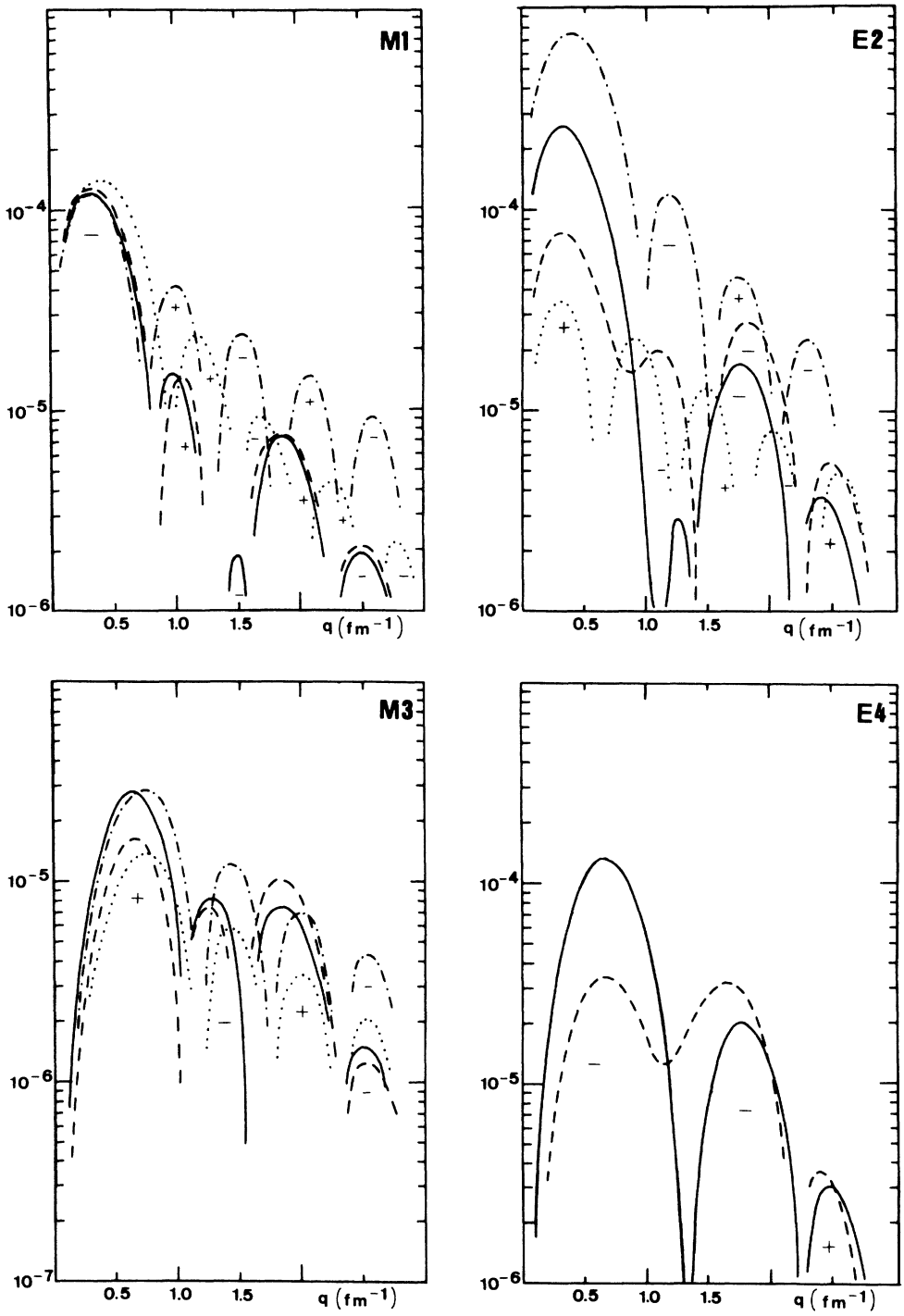

FIG. 9. Intrinsic $M1, M3$ and transition $E2, E4$ form factors of ^{154}Sm in PHF (——) and cranking (— — —) compared to the results of the rigid rotor (· · ·) and irrotational fluid flow (—·—·—·) models (see text).

$q > 0.9$ fm^{-1} the cranking result is always larger in magnitude than the PHF. (4) The $M3$ multipole shows a quite different structure in PHF than in cranking (except for ^{154}Sm) as well as in different nuclei. However, its main strength is in all cases similar, and is spread over the range $0.5 < q < 2$ fm^{-1}. As remarked upon in Sec. III B, the strong differences observed at $q < 0.6$ fm^{-1} for different nuclei come about mainly by a reduction in the convection contribution. (This reduction is linked to that of the hexadecupole moment, seen in Table III.) (5) For the $E4$ form factor, the first peak at $q \sim 0.6$ fm^{-1} is larger by a factor of 3 in PHF. As the nuclear mass increases, this peak is displaced towards larger q values and reduced in strength as the hexadecupole moment decreases. At $q > 1.3$ fm^{-1} both PHF and cranking results are closer, the latter being larger.

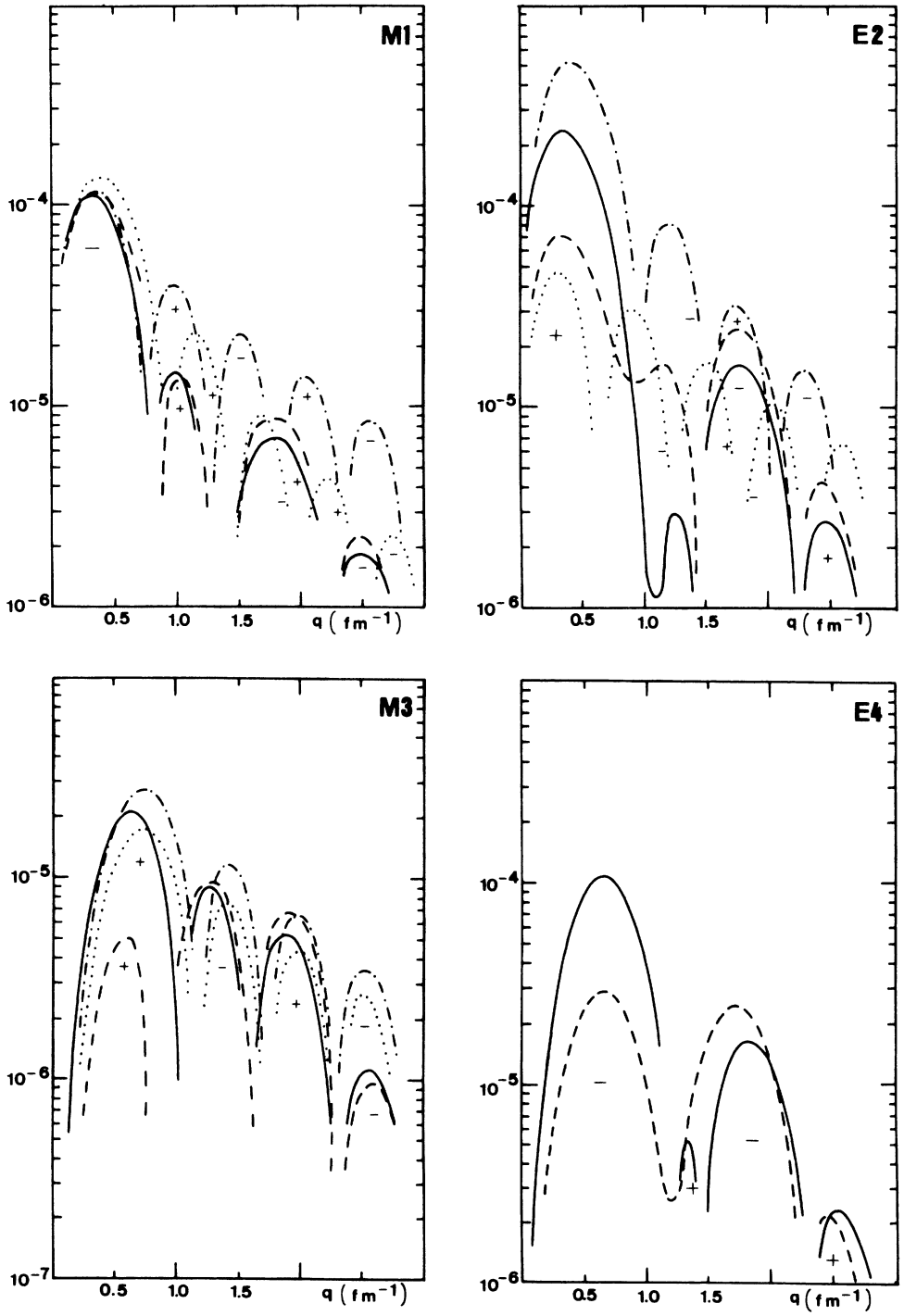

FIG. 10. Same as Fig. 9, for ^{158}Gd.

Concerning the comparison to macroscopic models, the following principal features are observed: (1) For all multipoles the q dependence of the microscopic models deviates substantially from the simple prescriptions of the IF and RR models expressed in Eqs. (9)–(11). The manner of this deviation depends on the particular nucleus and expresses the microscopic structure of the nucleus. In general, the dependence on nuclear structure is more pronounced for the cranking than for the PHF model. (2) The stronger model dependence is observed systematically in the $E2$ multipole. The first peak of the PHF or cranking model always falls between the IF and RR peaks, and the ratio of their maximum strengths is $(E2)_{\mathrm{IF}}/(E2)_{\mathrm{RR}} \simeq 15-20$. (3) On the other hand, the first peak of the $M1$ multipole is very close in all the models, both in position and in strength. The IF model in partic-

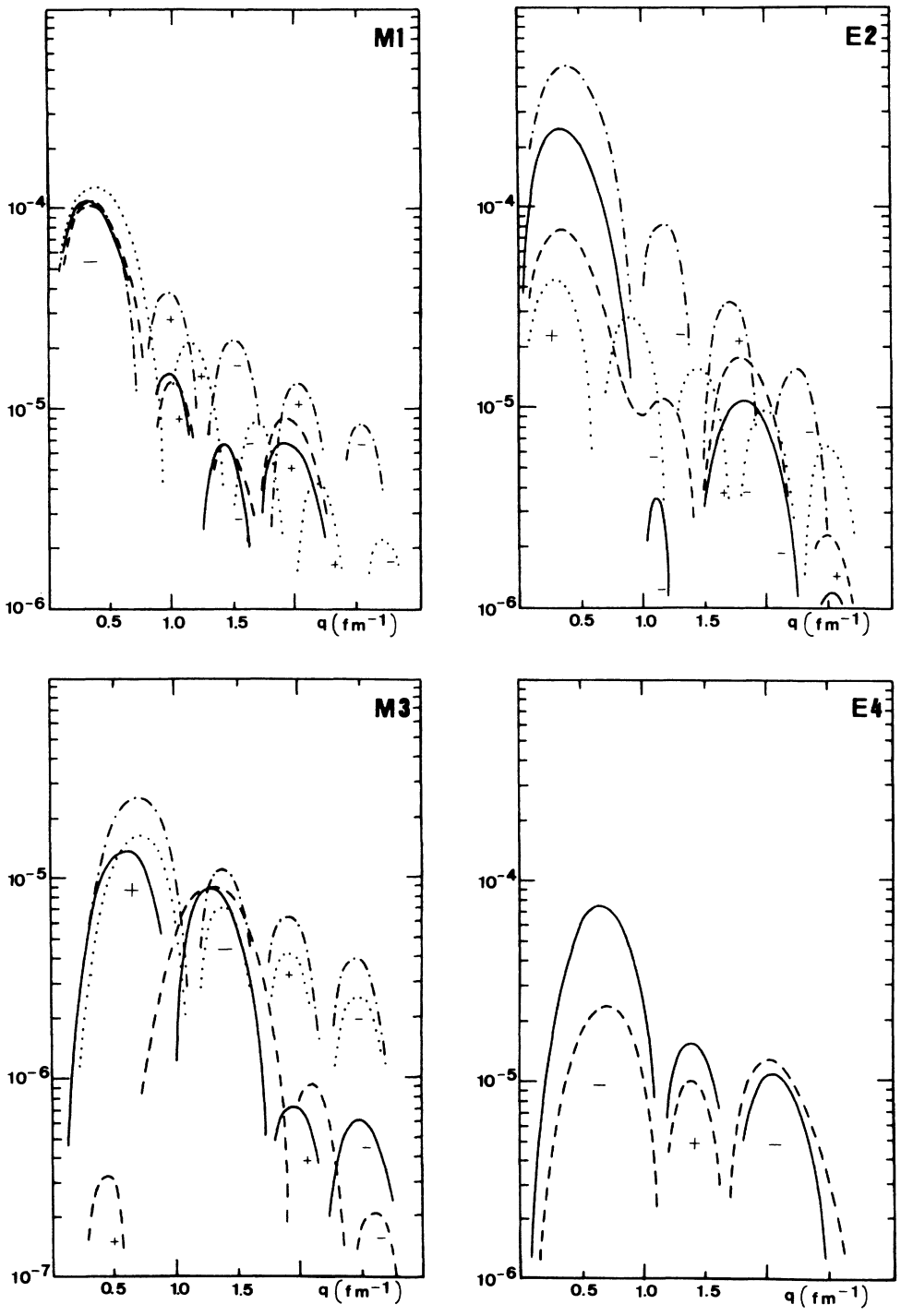

FIG. 11. Same as Fig. 9, for ^{164}Dy.

ular predicts quite accurately the first peak obtained by the microscopic models. Although the IF and RR predictions for $M1$ coincide at low $q < 1.5$ fm^{-1}, their different q dependencies show up already in the position and width of the peak, the RR model giving a slightly higher and broader peak.

The relationship between the PHF and cranking results can be further elucidated by inspection of Eqs. (3)–(6). As pointed out in Ref. 3, the PHF result can be interpreted as an "average" cranking model result. One can define an average inverse two-quasiparticle energy value $1/\bar{E}$ such that Eq. (6) can be written

$$\mathcal{J}_{\rm cr} = \langle J_\perp^2 \rangle / \bar{E} \ . \tag{21}$$

By analogy, one can define an average excitation energy $[\bar{E}_{\sigma\lambda}(q)]$ for the two-quasiparticle states contributing to each $\sigma\lambda$ multipole at a given q value, in the cranking

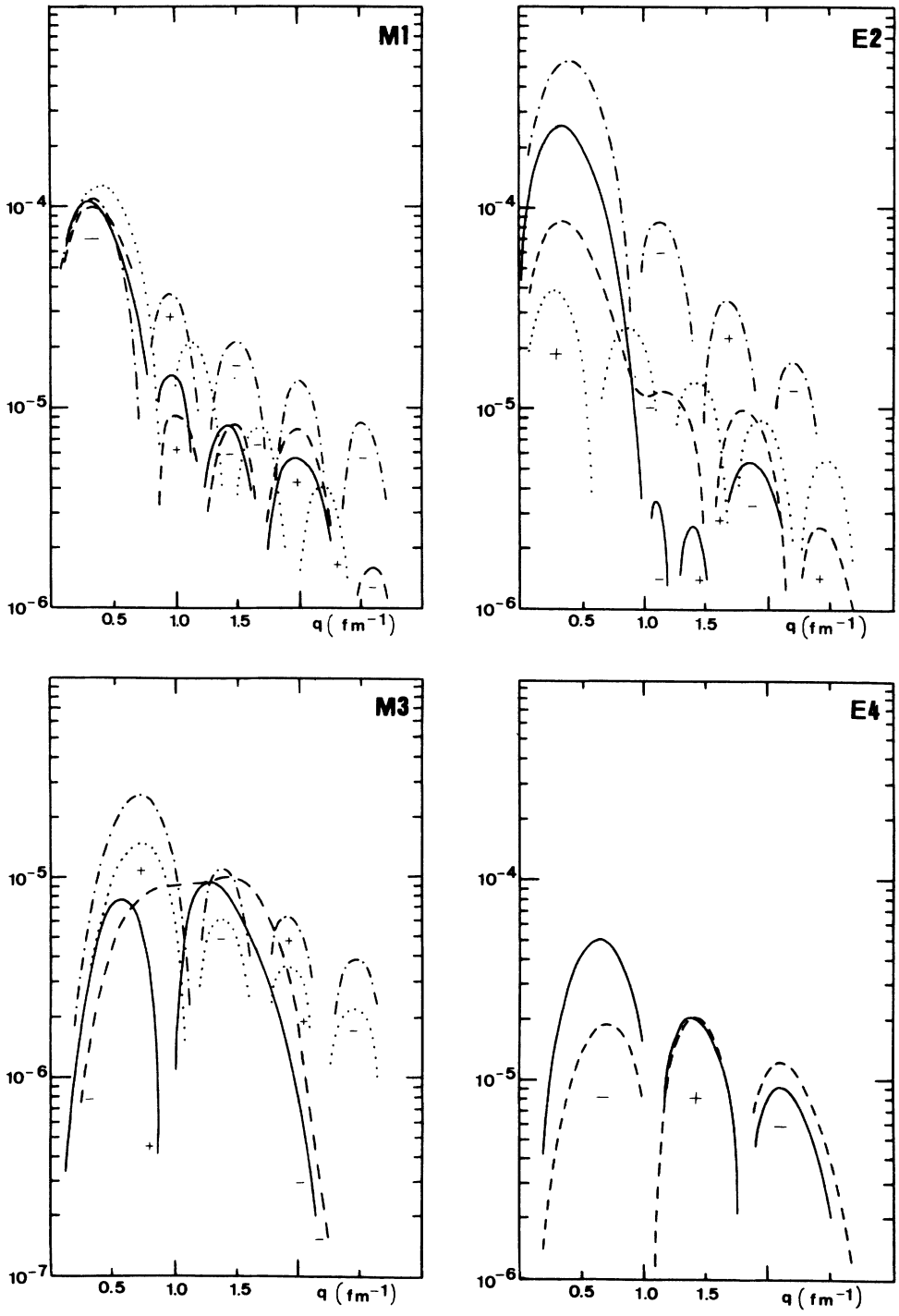

FIG. 12. Same as Fig. 9, for ^{168}Er.

model. Then comparing Eqs. (3), (4), and (21) we may write

$$[\mathcal{F}_R^{\sigma\lambda}(q)]_{\rm cr}=[\mathcal{F}_R^{\sigma\lambda}(q)]_{\rm PHF}\bar{E}/\bar{E}_{\sigma\lambda}(q) . \quad (22)$$

The PHF and cranking results will coincide at any q and for any multipole only if $\bar{E}_{\sigma\lambda}(q)=\bar{E}$. In this sense the PHF model can be interpreted as an approximation to the cranking model. The results will agree when the states $|\nu\rangle$ which contribute to Eq. (3) have similar excitation energies as those states which contribute to $\mathcal{I}_{\rm cr}$, and this depends both on the momentum transfer and on how similar the operator $T^{\sigma\lambda}$ is to the angular momentum operator. In view of the Wigner-Eckart theorem for vector operators, one understands why the $M1$ multipole and in particular its low momentum limit g_R, are so close in the two models. It is not surprising that higher multipoles show a much stronger model dependence.

For instance, with the Sk-3 force, the $\bar{E}$ value defined in Eq. (21) is approximately 5 MeV in all nuclei (see Table IV). Then, the fact that the first peak of the $E2$ (or $E4$) multipole is three times larger in PHF than in cranking implies that at low q values the average excitation energy of the intermediate states contributing to the $E2$ multipole is $\bar{E}_{E2}(q\sim 0.6)\simeq 15$ MeV $\simeq 3\bar{E}$. A ratio of order three can be understood on the basis that at low q, the single-particle states α,β contributing to $E2$ are located on the surface of the nucleus, and these tend to be the valence states of higher excitation energy. From similar arguments one can also understand why for this same multipole the cranking result is larger than the PHF at higher q. The difference between the two models lies in the fact that in PHF all intermediate states are weighted equally, while in cranking they are weighted inversely to their excitation energy.

The regularity in strength of the first peaks of the $M1$ and $E2$ multipoles for different nuclei, in both PHF and cranking, is consistent with the trend of their gyromagnetic ratios g_R and their $Q_2/\mathcal{I}_{\rm cr}$ ratios, respectively (see Tables III and IV). Note that at low-q, $\mathcal{F}_R^{M1}(q)$ and $\mathcal{F}_R^{E2}(q)$ are linear in q and must be proportional to g_R/Z and $Q_0/(\mathcal{I}Z)$, respectively [see Eqs. (7) and (8)]. Although strictly speaking Eqs. (7) and (8) hold only in the narrow range $q<0.1$ fm^{-1}, one sees in Figs. 6–12 that the strength of the first $M1$ peak is indeed roughly proportional to the g_R value of Table IV, for the corresponding nuclei and models. For the transverse electric form factors we note that Eq. (7) follows from current conservation (cc).

Assuming a purely rotational spectrum, $E_I\sim I(I+1)/2\mathcal{I}$, cc implies that at low q,

$$\mathcal{F}_R^{E\lambda}(q)=\frac{-i^\lambda}{2(2\lambda-1)!!}\sqrt{\lambda+1/\lambda(2\lambda+1)}\frac{Q_\lambda}{2\mathcal{I}Z}q^{\lambda-1} , \quad (23)$$

when $qR_0\ll 1$. According to Ref. 17, within either of the macroscopic models (IF and RR), cc is satisfied. This implies that at low q the $\mathcal{F}_R^{E\lambda}(q)$ values given by the IF (RR) model are exactly those of Eq. (23) with Q_λ and $\mathcal{I}$ the IF (RR) values. In the present work we have used the experimental values for the intrinsic quadrupole moment ($Q_2\equiv Q_0$) and neglected hexadecupole deformations. In this approximation one has

$$[\mathcal{F}_R^{E2}(q)]_{\rm IF}/[\mathcal{F}_R^{E2}(q)]_{\rm RR}=\mathcal{I}_{\rm RR}/\mathcal{I}_{\rm IF} . \quad (24)$$

This ratio is of order 13 for a typical deformation $\beta\sim 0.3$. On the other hand, at larger $q>0.1$ fm^{-1}, the q dependence of the $E2$ multipole is different in the two models [see Eqs. (10a) and (10b)] and tends to increase the ratio from the value given in Eq. (24) at $q\sim 0.25$ where the main peak occurs, as can be seen in Figs. 9–12. The ratio between the maximum strengths is of the order of 20. As is well known, the RR and IF models provide upper and lower limits to the moment of inertia: $\mathcal{I}_{\rm RR}>\mathcal{I}_{\rm exp}>\mathcal{I}_{\rm IF}$. Therefore, the $[\mathcal{F}_R^{E2}(q)]_{\rm RR}$ and $[\mathcal{F}_R^{E2}(q)]_{\rm IF}$ form factors can be interpreted as lower and upper bounds to the experimental $E2$ form factor, at least in the low-q region $q\lesssim 1.0$ fm^{-1}. It is no surprise that the results of the microscopic models, being more realistic, fall in between these two extremes. For the $M1$ multipole the IF and RR models give identical results for $q<2/R_0$, but differ in their q dependence at larger q, as shown in Eqs. (9a) and (9b).

Current conservation is approximately satisfied in the cranking model, but not in PHF. In addition, the cranking moments of inertia are close[3] to the experimental values (see Table IV). Therefore one expects the cranking model to be a better approximation to the $E\lambda$ multipoles. That this is indeed the case can be seen in Table V, where we compare the different model predictions for $\mathcal{F}_R^{E2}$ ($q=0.2$ MeV/c) at very low q, to experimental values. The latter have been obtained via Eq. (7) using experimental values for Q_0 and $\mathcal{I}$.[34] For completeness Table V

TABLE V. Experimental and calculated values of $\mathcal{F}_R^{M1}(q)$ and $\mathcal{F}_R^{E2}(q)$ at $q=0.2$ MeV/c. The results quoted for PHF and cranking models are for the Sk-3 force.

	$\mathcal{F}_R^{M1}(q)\times 10^7$				$\mathcal{F}_R^{E2}(q)\times 10^8$				
Nucleus	Exp	cr	PHF	RR,IF	Exp	cr	PHF	RR	IF
^{154}Sm	−4.78±0.71	−5.80	−5.82	−5.57	4.85±0.16	6.20	19.6	3.03	47.0
^{156}Gd	−4.76±0.68	−4.77	−5.44	−5.50	7.6±1.3	5.22	18.0	3.57	38.2
^{158}Gd	−4.97±0.62	−5.11	−5.46	−5.43	6.27±0.22	5.70	18.6	3.72	35.6
^{164}Dy	−4.62±0.27	−4.55	−5.11	−5.23	6.35±0.03	5.80	18.8	3.49	35.3
^{166}Er	−4.16±0.19	−4.32	−5.01	−5.17	7.5±1.5	6.05	19.1	3.36	35.9
^{168}Er	−3.97±0.51	−4.44	−4.98	−5.10	6.82±0.06	6.29	18.9	3.32	35.5
^{174}Yb	−3.67±0.56	−3.81	−4.69	−4.93	6.43±0.04	5.65	17.0	3.29	33.3

includes predictions for $\mathcal{F}_R^{M1}$ ($q=0.2$ MeV/c) together with experimental values from Eq. (8) (see also Table IV). It is clear from Table V that for every model, agreement with experiment is better for the $M1$ multipole than for the $E2$. In the $M1$ case, there is no constraint from current conservation which can be used to prefer one model over another. It is then reassuring to see that the different models agree so well in the $M1$ case, so that one may take microscopic $M1$ results from Figs. 6–12 as reliable predictions, particularly so for the main peak.

IV. CONCLUSION

An extensive, systematic study of collective rotational transverse current multipoles of the ground-state band of even-even rare-earth nuclei has been presented. We have compared the results from HF+BCS (Sk-3 and Ska) and Nilsson wave functions on the one hand, using both the PHF and cranking models, with those from the macroscopic IF and RR models. For the M1 multipole we find rather similar results at low q, for all the models considered, and fair agreement with the limited experimental data available. This implies that at least in the first peak of the M1 form factor, where convection contributions are dominant, one can have confidence in the results of the microscopic models, and even the simpler models give reliable estimates.

For the other multipoles, there is much greater dependence on the model, on the mean field, and on the nucleus considered. Nilsson wave functions were seen to give larger high momentum components than do HF wave functions. That current conservation is satisfied by the cranking model gives us greater confidence in this model for the $E2$ and $E4$ multipoles. In the $E2$ case, a strong dependence on the model is found; in the limit $q\rightarrow 0$ the cranking result agrees better with experiment. The IF and RR models provide upper and lower bounds, when $q<1$ fm^{-1}, for the microscopic model results. The $E4$ multipole depends much more strongly on the nucleus than does $E2$, reflecting a sensitivity to the hexadecupole moment, which changes by nearly an order of magnitude in going from ^{154}Sm to ^{174}Yb. Results for the $M3$ multipole are highly variable, and it is difficult to identify any systematic trends.

It will be particularly interesting, in future, to see what experiment provides, and so identify which calculation is the most realistic. We hope that this survey and comparison will be useful in indicating which features of a given calculational scheme are typical, and which are particular to the model and nucleus considered. As experimental results become available there will be much to learn from such comparisons.

ACKNOWLEDGMENTS

We are grateful to Prof. S. Kowalski for providing us with a copy of his PHF code and for advice in its utilization. We are grateful to the Natural Sciences and Engineering Research Council of Canada for continued support under operating Grant No. A-3198. Two of us (E.M.G. and P.S.) are indebted to La Comisión Asesora de Investigación Científica y Técnica of Spain, for partial financial support under Grant No. PR84-1179, and to the Theory Group of the Physics Department of McMaster University for their kind hospitality. P.S. thanks the University of Extremadura for financial support during his Ph. D. studies, and the Consejo Superior de Investigaciones Científicas (Spain) for the award of a post-doctoral fellowship tenable at McMaster.

*Present address: Department of Physics and Astronomy, Rutgers University, P.O. Box 849, Piscataway, N.J. 08854.

†Permanent address: Instituto de Estructura de la Materia, Consejo Superior de Investigaciones Científicas, Serrano 119, 28006 Madrid, Spain.

‡Permanent address: Kyocera Corp., Central Research Lab., CAT Centre, 1-4 Yamashita-Cho, Kokubu, Kagoshima 899-43, Japan.

[1]J. Rainwater, Phys. Rev. **79**, 432 (1950); A. Bohr and B. R. Mottelson, Mat. Fys. Medd. Dan. Vid. Selsk. **27**, No. 16 (1953).

[2]O. Prior, F. Boehm, and S. G. Nilsson, Nucl. Phys. **A110**, 257 (1968).

[3]D. W. L. Sprung, S. G. Lie, M Vallieres, and P. Quentin, Nucl. Phys. **A326**, 37 (1979).

[4]S. Frauendorf, in *Proceedings of the Nuclear Physics Workshop of the International Centre for Theoretical Physics, Trieste, 1981,* edited by C. H. Dasso, (North-Holland, Amsterdam, 1982), p. 111–130.

[5]D. Bohle, A. Richter, U. E. P. Berg, J. Drexler, R. D. Heil, U. Kneissl, H. Metzger, R. Stock, B. Fischer, H. Hollick, and D. Kollewe, Nucl. Phys. **A458**, 205 (1986).

[6]M. Radomski, Phys. Rev. C **14**, 1704 (1976); P. Gulshani and D. J. Rowe, Can. J. Phys. **56**, 468 (1978); **56**, 480 (1978); J. Fleckner, J. Kunz, U. Mosel, and E. Wüst, Nucl. Phys. **A339**, 227 (1980).

[7]E. Moya de Guerra and A. E. L. Dieperink, Phys. Rev. C **18**, 1596 (1978).

[8]E. Moya de Guerra and S. Kowalski, Phys. Rev. C **22**, 1308 (1980); **20**, 357 (1979).

[9]E. Moya de Guerra, Ann. Phys. (N.Y.) **128**, 286 (1980).

[10]J. W. Negele and D. Vautherin, Phys. Rev. C **5**, 1472 (1972); **11**, 1031 (1975).

[11]E. Moya de Guerra, Nucl. Phys. **A366**, 259 (1981).

[12]E. Wüst, U. Mosel, J. Kunz, H. G. Andresen, and M. Müller, Nucl. Phys. **A402**, 235 (1983).

[13]T. W. Donnelly and I. Sick, private communication.

[14]T. W. Donnelly and E. Moya de Guerra (unpublished).

[15]A. E. L. Dieperink and E. Moya de Guerra, Phys. Lett. **B189**, 267 (1987).

[16]M. Nishimura, D. W. L. Sprung, and E. Moya de Guerra, Phys. Lett. **161B**, 235 (1985); Nucl. Phys. **A435**, 523 (1985); P. Sarriguren and E. Moya de Guerra, Phys. Rev. C **30**, 2105 (1984).

[17]E. Moya de Guerra, Phys. Rep. **138(6)**, 293 (1986).
[18]T. de Forest and J. D. Walecka, Adv. Phys. **15**, 1 (1966).
[19]T. W. Donnelly and J. D. Walecka, Ann. Rev. Nucl. Sci. **25**, 329 (1975).
[20]D. R. Inglis, Phys. Rev. **96**, 1059 (1954); **97**, 701 (1955).
[21]A. Bohr and B. Mottelson, *Nuclear Structure* (Benjamin, New York, 1975), Vol. 2.
[22]A. Richter, in *Nuclear Structure 1985,* Proceedings of the Niels Bohr Centennial Conference, edited by R. Broglia, G. Hagemann, B. Hersind (North-Holland, Amsterdam, 1985), and references therein.
[23]F. Beiner, H. Flocard, N. Van Giai, and P. Quentin, Nucl. Phys. **A238**, 29 (1975).
[24]H. S. Köhler, Nucl. Phys. **A258**, 301 (1976).
[25]D. Vautherin, Phys. Rev. C **7**, 296 (1973).
[26]P. Sarriguren, Ph. D. thesis, University of Extremadura, Badajoz, Spain, 1987.
[27]V. Bernard and C. Mahaux, Phys. Rev. C **23**, 888 (1981); C. Mahaux and H. Ngo, Phys. Lett. **100B**, 285 (1981).
[28]H. Flocard, P. Quentin and D. Vautherin, Phys. Lett. **46B**, 304 (1973); P. Bonche, H. Flocard, P. H. Heenen, S. J. Krieger, and M. S. Weiss, Nucl. Phys. **A443**, 39 (1985).
[29]F. Tondeur, D. Berdichevsky, and M. Farine, Z. Phys. **A325**, 405 (1986).
[30]M. Vallieres and D. W. L. Sprung, Can. J. Phys. **56**, 1190 (1978).
[31]P. Ring and P. Schuck, *The Nuclear Many-Body Problem,* (Springer-Verlag, New York, 1980), p. 29.
[32]G. G. Simon, Ch. Schmitt, F. Borkowski, and V. H. Walther, Nucl. Phys. **A333**, 381 (1980).
[33]H. Chandra and G. Sauer, Phys. Rev. C **13**, 245 (1976).
[34]C. M. Lederer and V. S. Shirley, *Table of Isotopes,* (Wiley, New York, 1978). See also S. Raman *et al.*, At. Nucl. Data Tables **36**, 1 (1987).